Electronic Supplementary Material (ESI) for Physical Chemistry Chemical Physics.
This journal is © the Owner Societies 2016

Supporting Information

Computational prediction and analysis of the ^{27}Al solid-state NMR spectrum of methylaluminoxane (MAO) at variable temperatures and field strengths

Zackary Falls,[1] Eva Zurek,[1] and Jochen Autschbach[1]

[1]*Department of Chemistry, University at Buffalo, State University of New York, Buffalo, NY 14260-3000, USA*

(Dated: July 8, 2016)

FIG. S1. SSNMR spectra of MAO at 398 K absent free TMA, simulated at different field strengths (the corresponding proton resonance frequencies are also provided). The Boltzmann averaged contributions to the spectra from h-h-h, s-h-h and s-s-h Al sites are given separately. Species with 3-coordinate, 4-coordinate, or h-h-o aluminum sites are not predicted to be stable at this temperature.

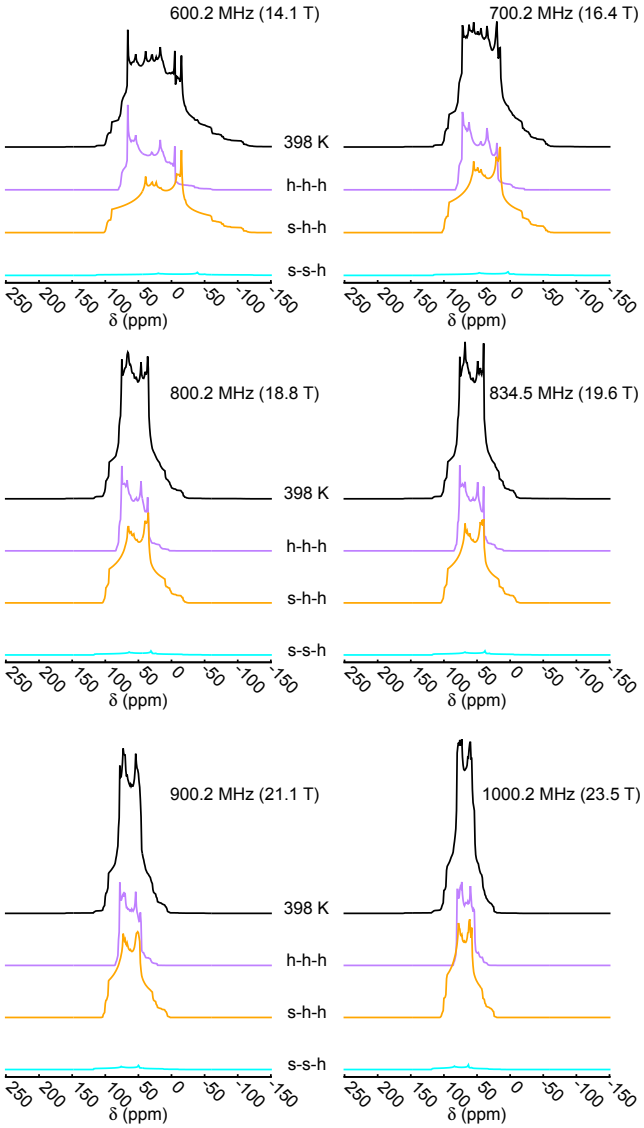

FIG. S2. SSNMR spectra of MAO at 498 K absent free TMA, simulated at different field strengths (the corresponding proton resonance frequencies are also provided). The Boltzmann averaged contributions to the spectra from Al sites are given separately. Species with 3-coordinate, 4-coordinate, or h-h-o aluminum sites are not predicted to be stable at this temperature.

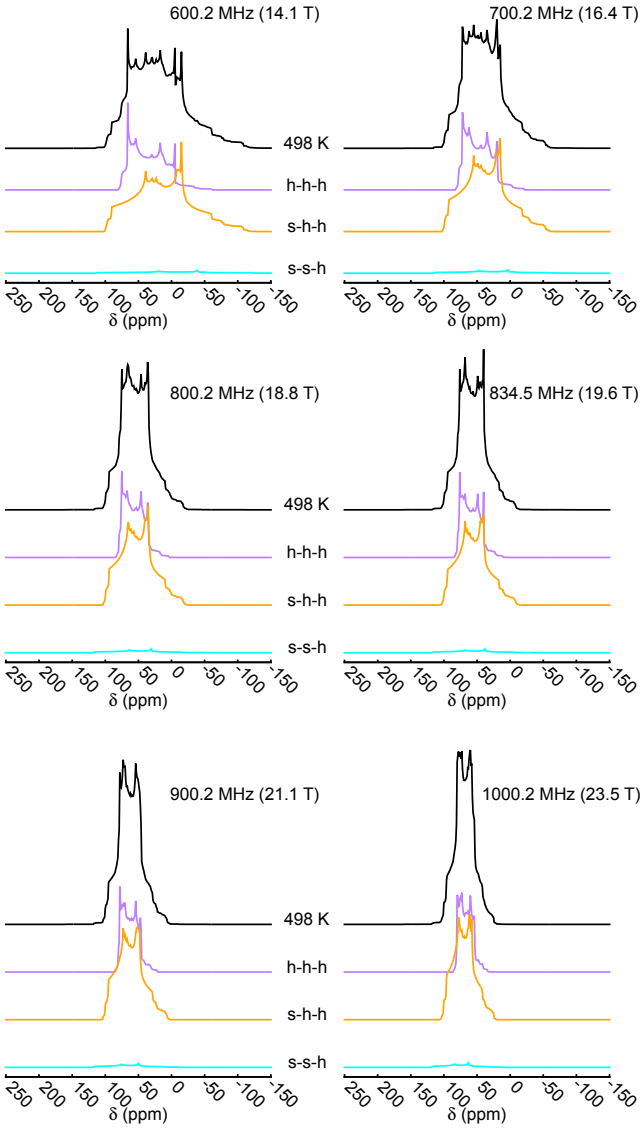

FIG. S3. SSNMR spectra of MAO at 77 K absent free TMA, simulated at different field strengths (the corresponding proton resonance frequencies are also provided) with various Gaussian broadening frequencies applied. The Boltzmann averaged contributions to the spectra from Al sites are given separately.

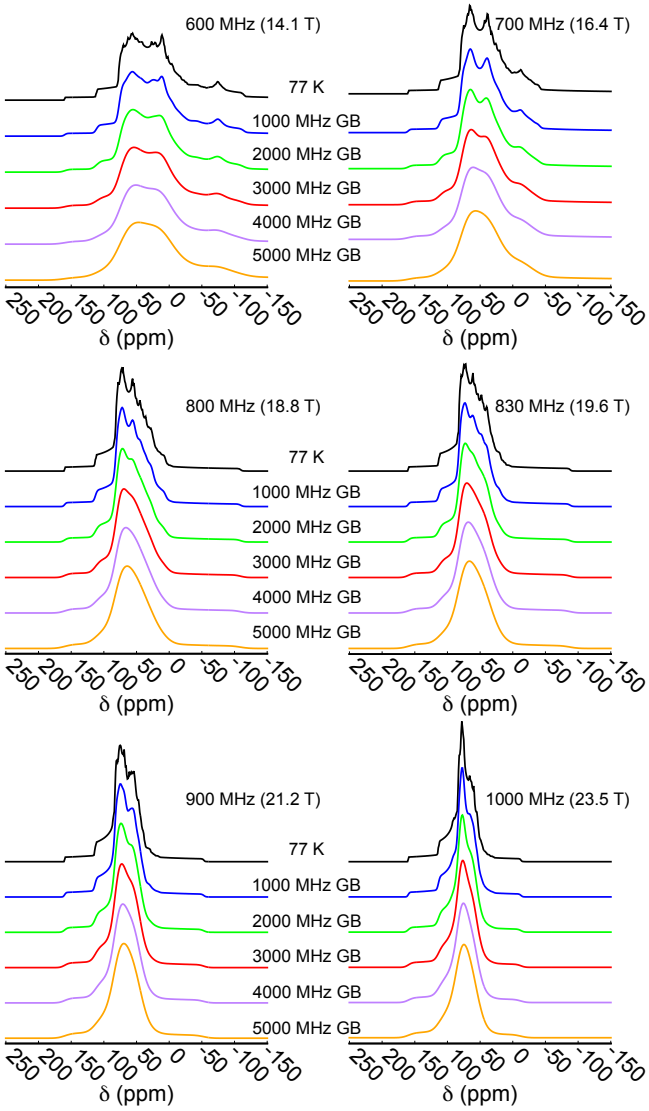

FIG. S4. SSNMR spectra of MAO at 298 K absent free TMA, simulated at different field strengths (the corresponding proton resonance frequencies are also provided) with various Gaussian broadening frequencies applied. The Boltzmann averaged contributions to the spectra from Al sites are given separately.

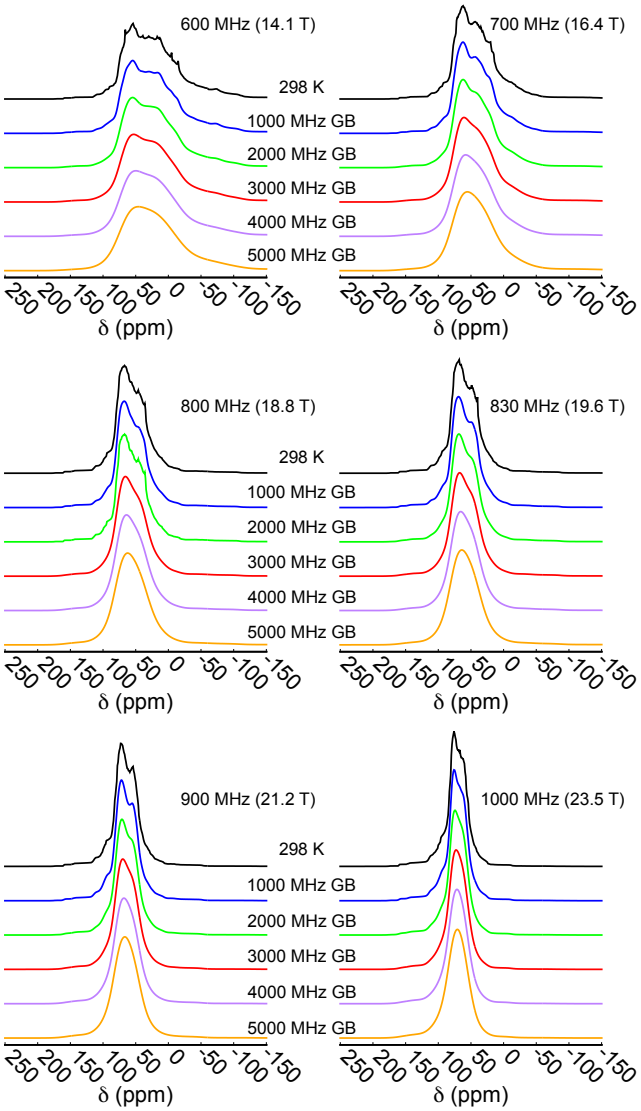

FIG. S5. SSNMR spectra of MAO at 398 K absent free TMA, simulated at different field strengths (the corresponding proton resonance frequencies are also provided) with various Gaussian broadening frequencies applied. The Boltzmann averaged contributions to the spectra from Al sites are given separately.

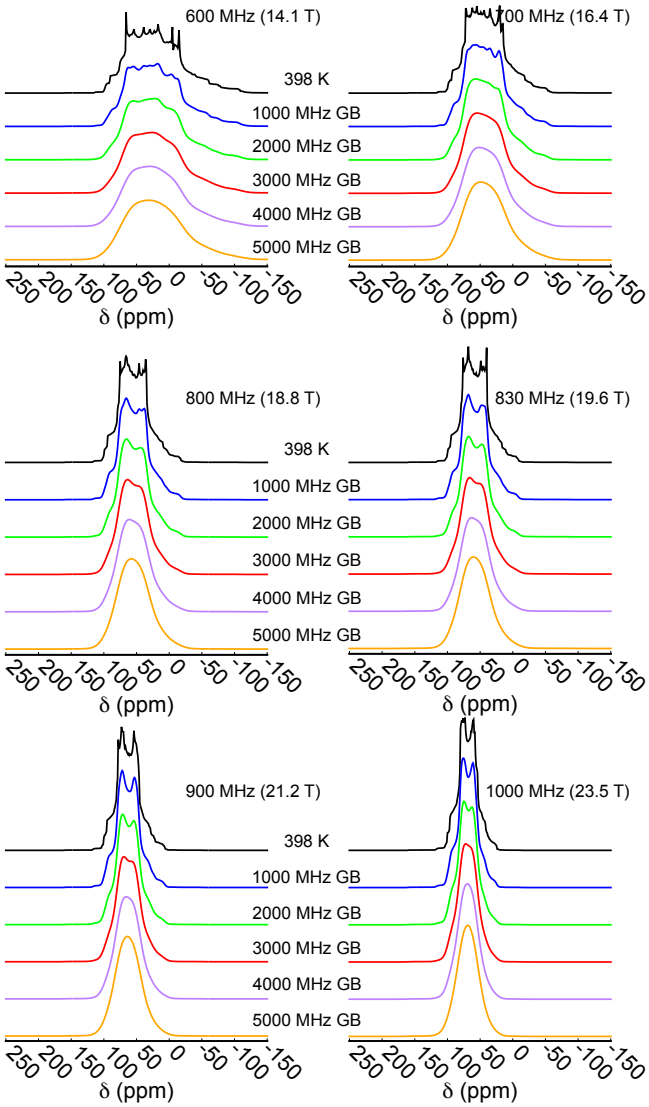

FIG. S6. SSNMR spectra of MAO at 498 K absent free TMA, simulated at different field strengths (the corresponding proton resonance frequencies are also provided) with various Gaussian broadening frequencies applied. The Boltzmann averaged contributions to the spectra from Al sites are given separately.

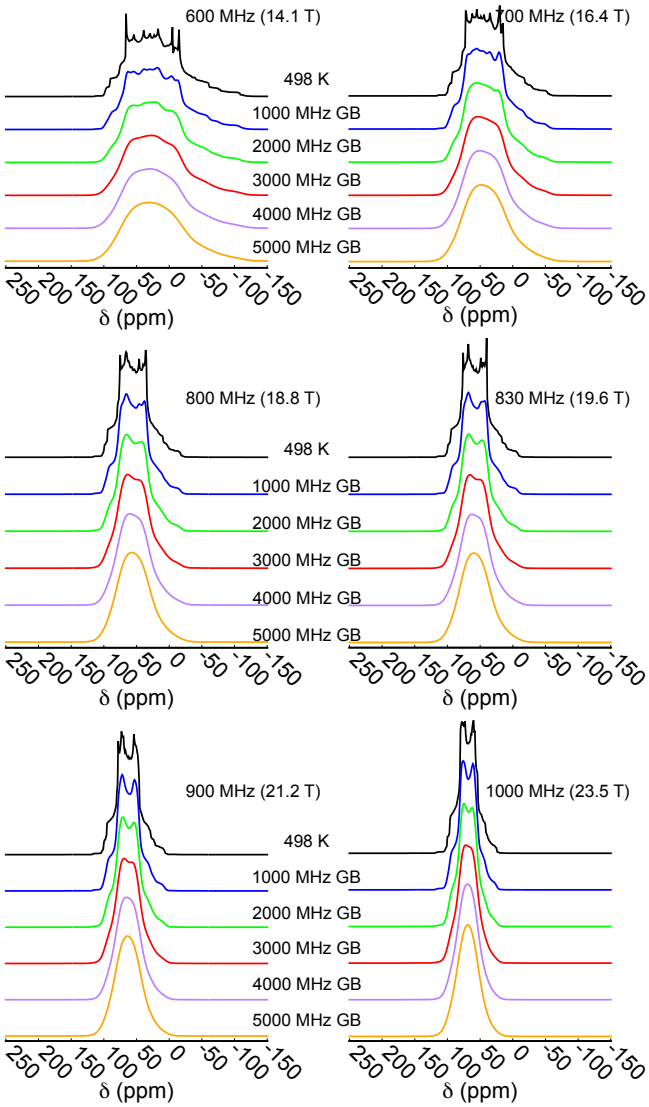

FIG. S7. SSNMR spectra of **$(AlMe_3)_2$ and $(AlMe_3)$**, simulated at different field strengths (the corresponding proton resonance frequencies are also provided).

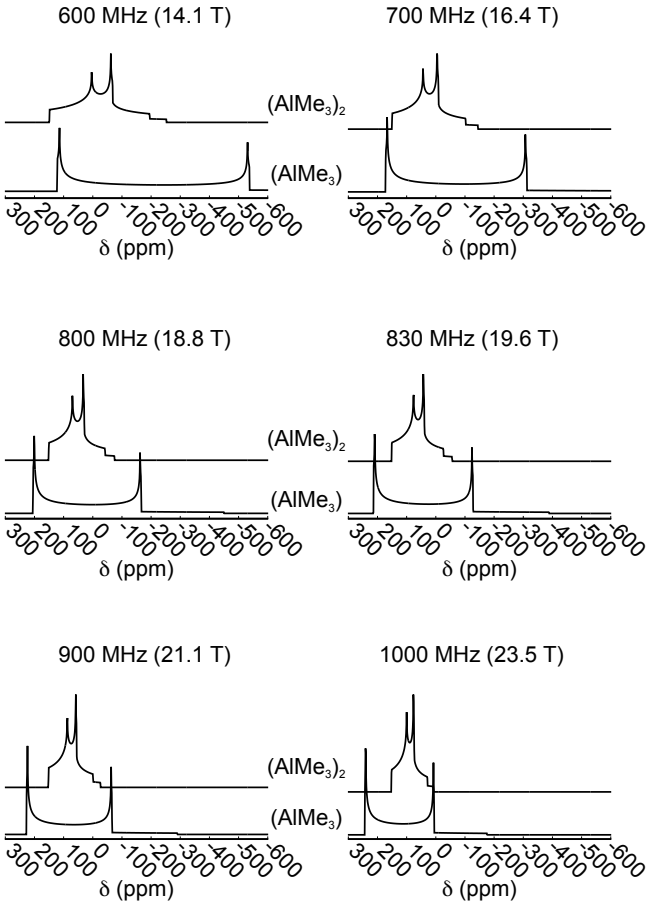

FIG. S8. Calculated EFG parameters and NMR chemical shifts of TMA monomer and dimer.

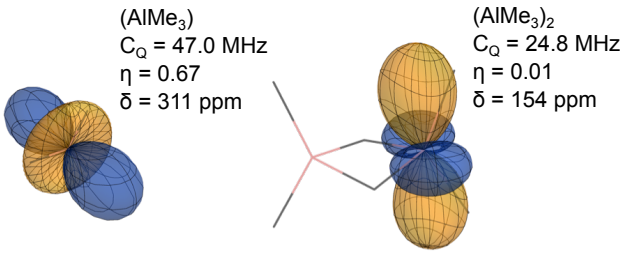

FIG. S9. SSNMR spectra of **(AlOMe)$_{6,c}$**, simulated at different field strengths (the corresponding proton resonance frequencies are also provided).

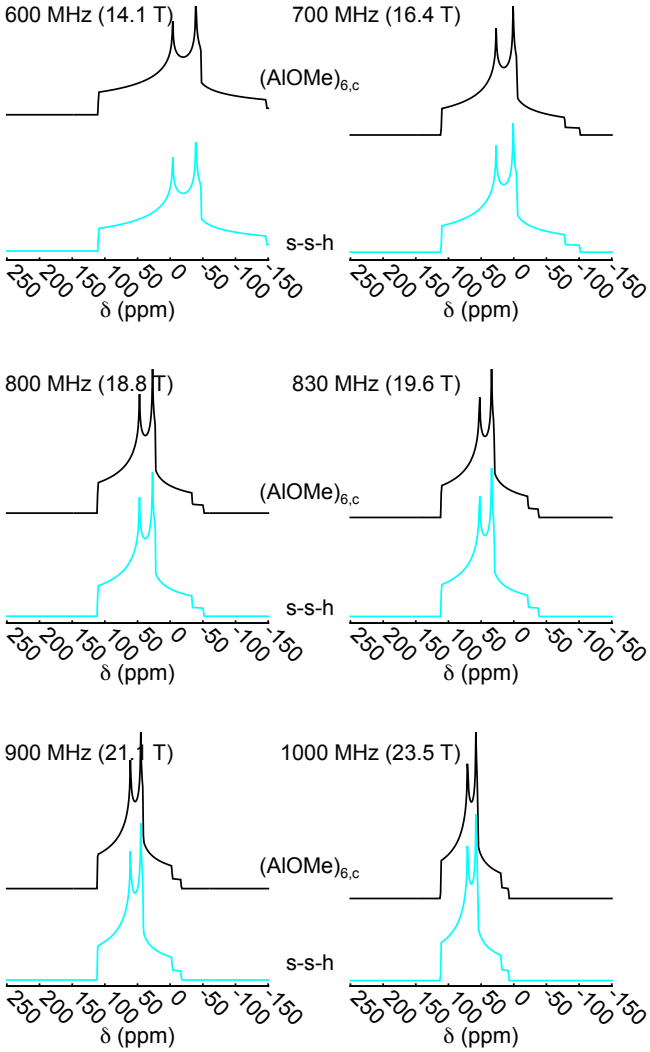

FIG. S10. Calculated EFG parameters and NMR chemical shifts of **(AlOMe)$_{6,c}$**.

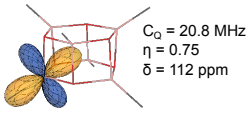

FIG. S11. SSNMR spectra of **(AlOMe)$_{6,c}$ · (AlMe$_3$)**, simulated at different field strengths (the corresponding proton resonance frequencies are also provided).

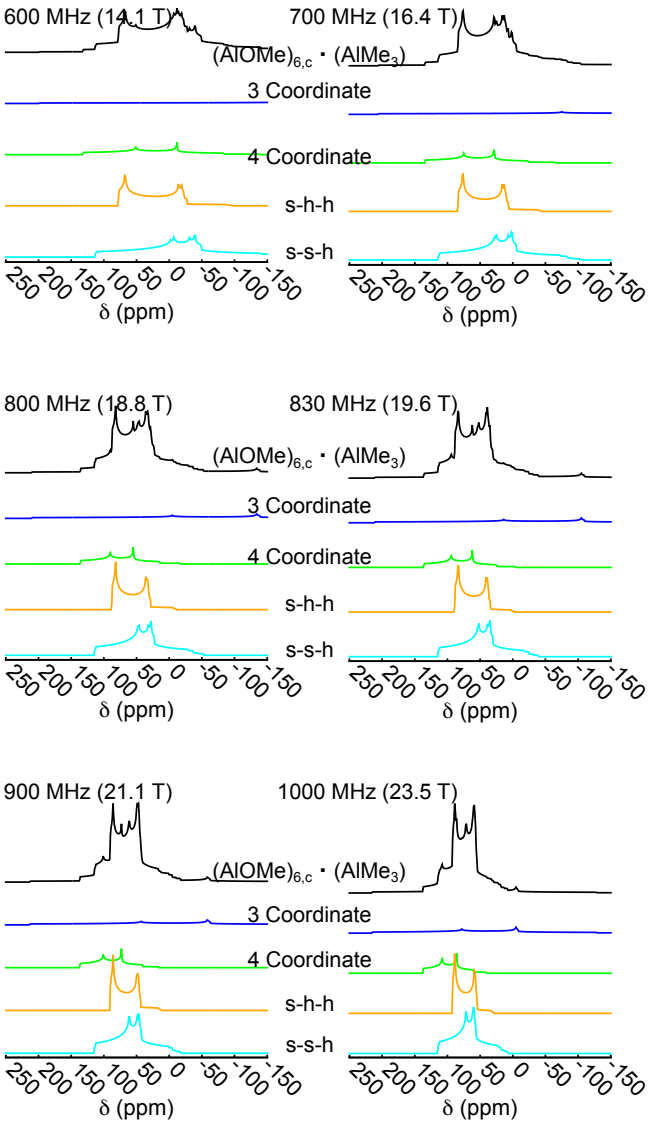

FIG. S12. Calculated EFG parameters and NMR chemical shifts of **(AlOMe)$_{6,c}$ · (AlMe$_3$)**.

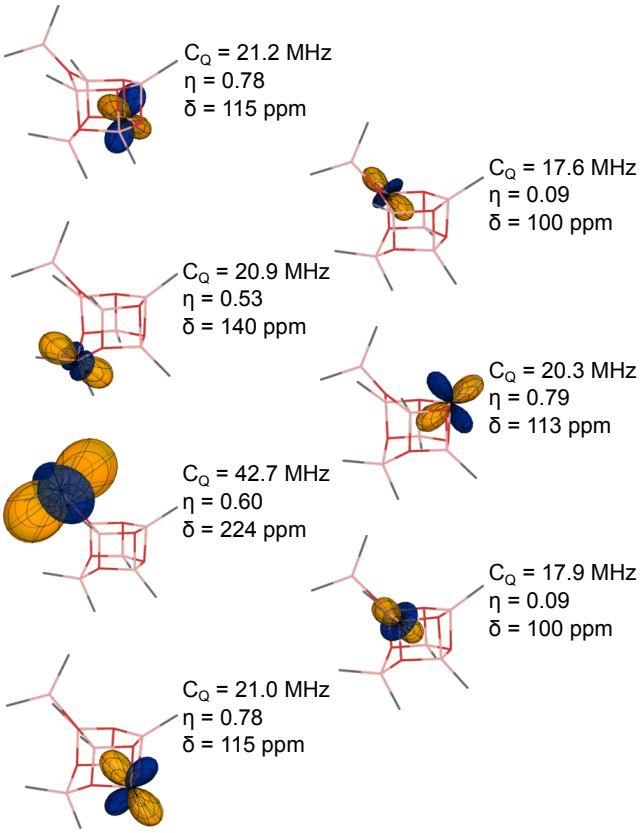

FIG. S13. SSNMR spectra of $\mathbf{(AlOMe)_{6,c} \cdot (AlMe_3)_2}$, simulated at different field strengths (the corresponding proton resonance frequencies are also provided).

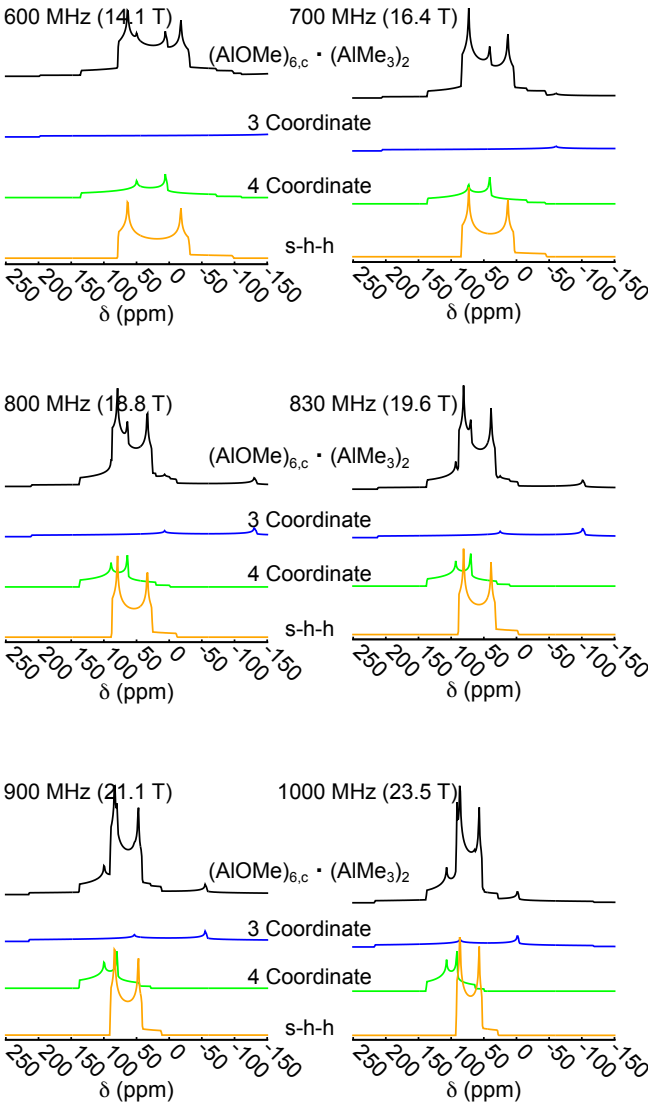

FIG. S14. Calculated EFG parameters and NMR chemical shifts of $\mathbf{(AlOMe)_{6,c} \cdot (AlMe_3)_2}$.

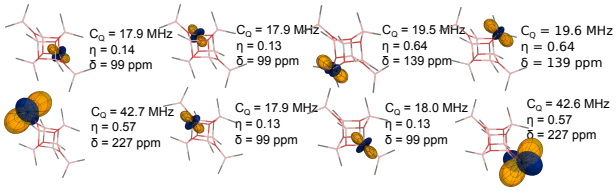

FIG. S15. SSNMR spectra of $\mathbf{(AlOMe)_{6,c} \cdot (AlMe_3)_3}$, simulated at different field strengths (the corresponding proton resonance frequencies are also provided).

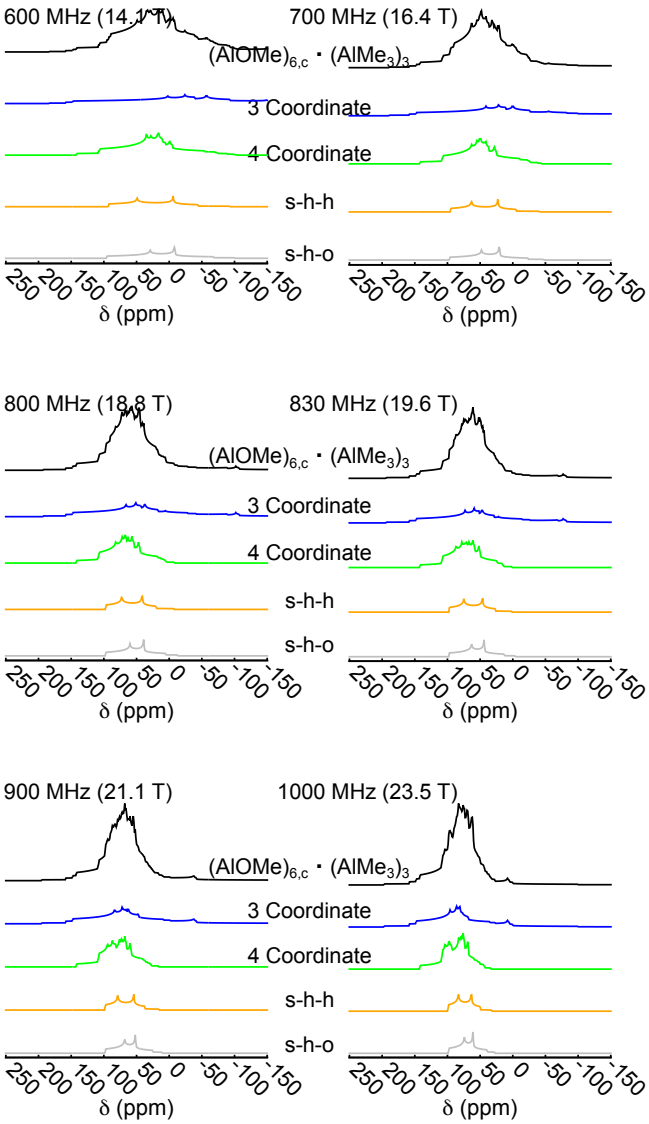

FIG. S16. Calculated EFG parameters and NMR chemical shifts of $\mathbf{(AlOMe)_{6,c} \cdot (AlMe_3)_3}$.

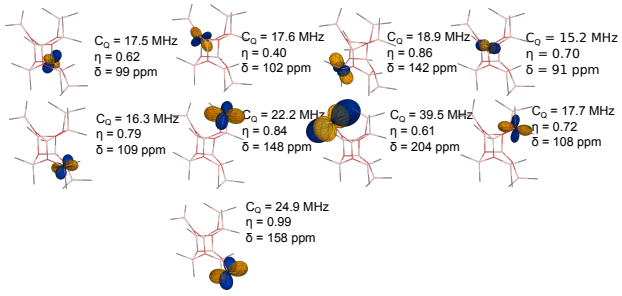

FIG. S17. SSNMR spectra of $\mathbf{(AlOMe)_{6,c} \cdot (AlMe_3)_4}$, simulated at different field strengths (the corresponding proton resonance frequencies are also provided).

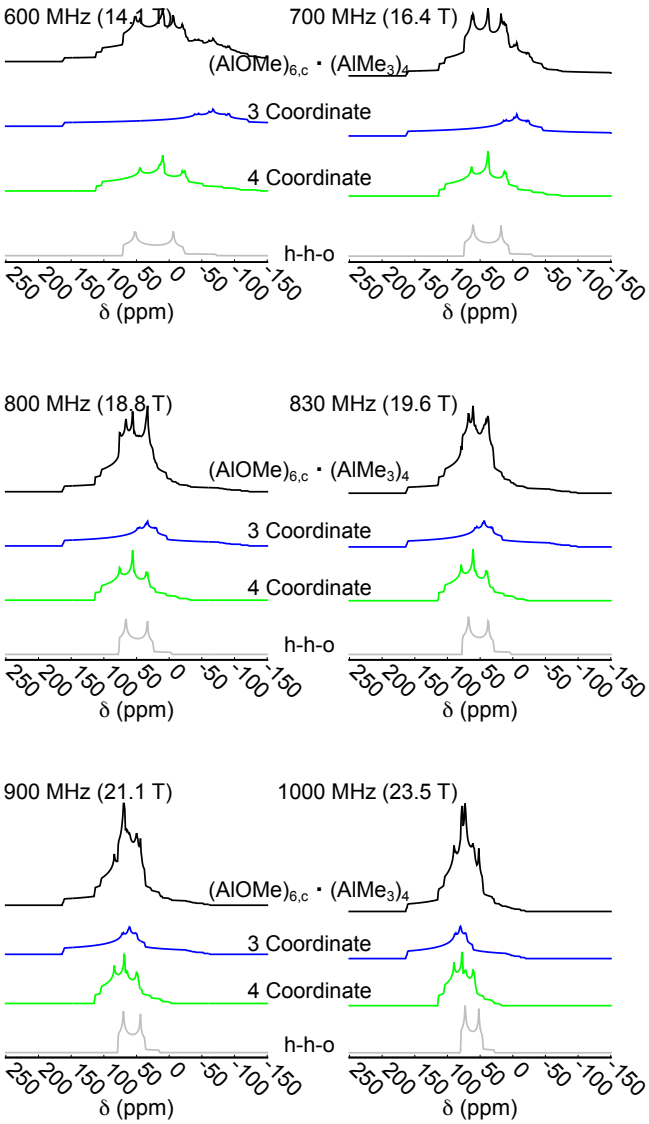

FIG. S18. Calculated EFG parameters and NMR chemical shifts of $\mathbf{(AlOMe)_{6,c} \cdot (AlMe_3)_4}$.

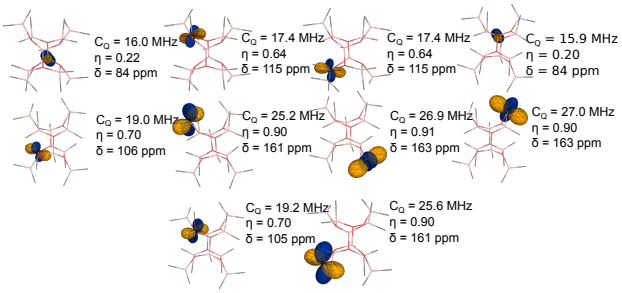

FIG. S19. SSNMR spectra of **(AlOMe)$_{8,c}$**, simulated at different field strengths (the corresponding proton resonance frequencies are also provided).

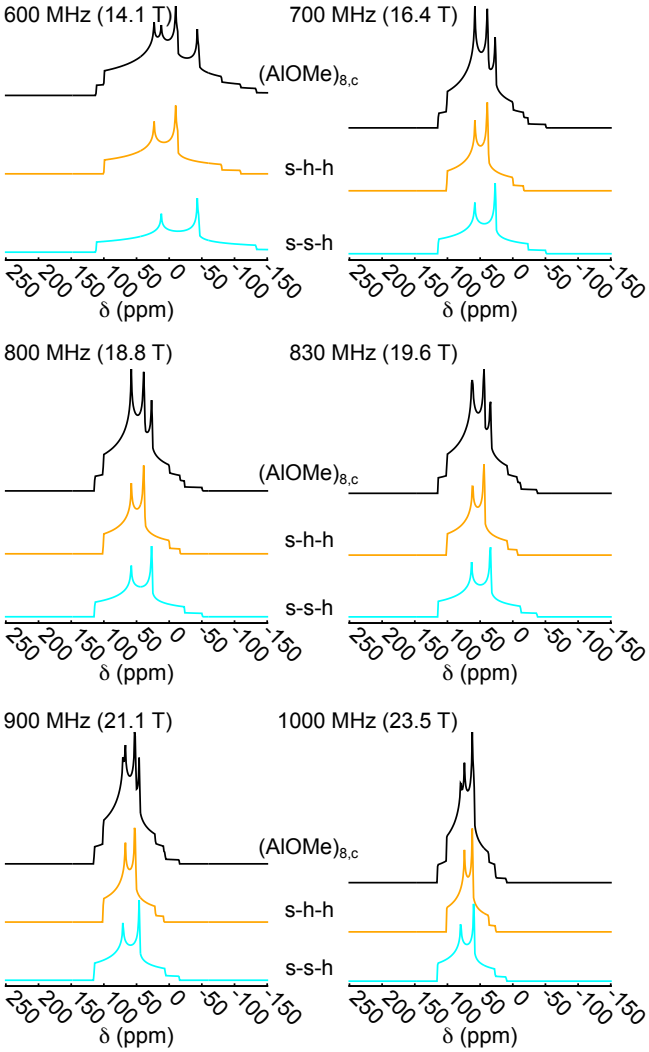

FIG. S20. Calculated EFG parameters and NMR chemical shifts of **(AlOMe)$_{8,c}$**.

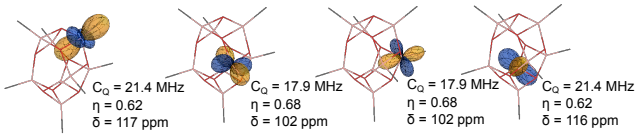

FIG. S21. SSNMR spectra of **(AlOMe)$_{8,c}$ · (AlMe$_3$)**, simulated at different field strengths (the corresponding proton resonance frequencies are also provided).

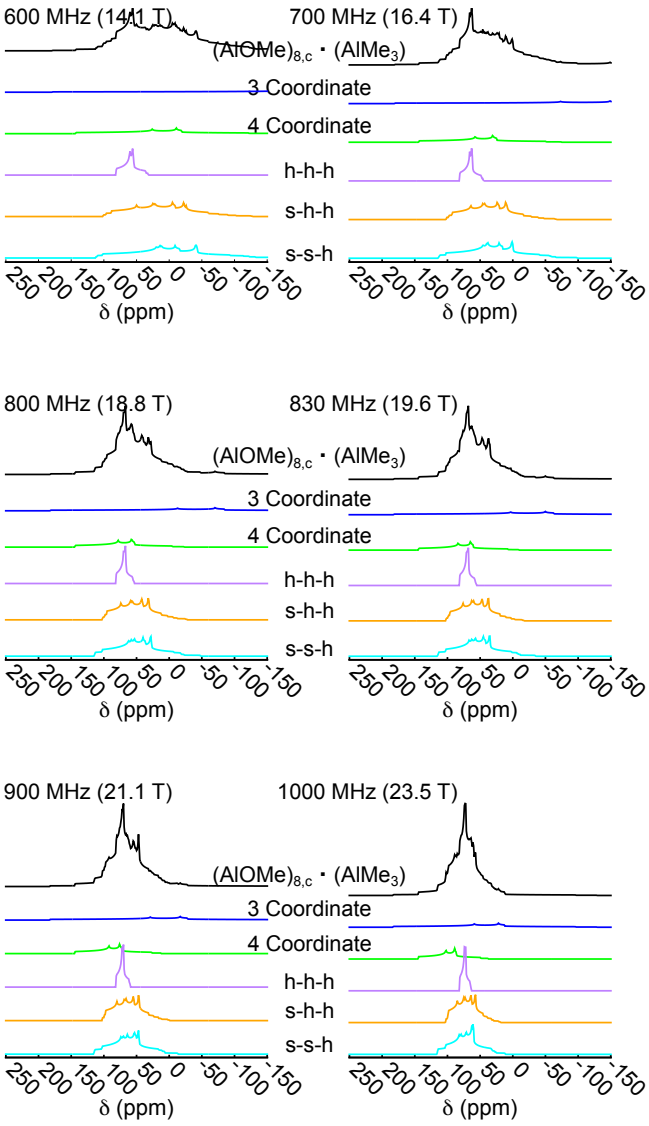

FIG. S22. Calculated EFG parameters and NMR chemical shifts of **(AlOMe)$_{8,c}$ · (AlMe$_3$)**.

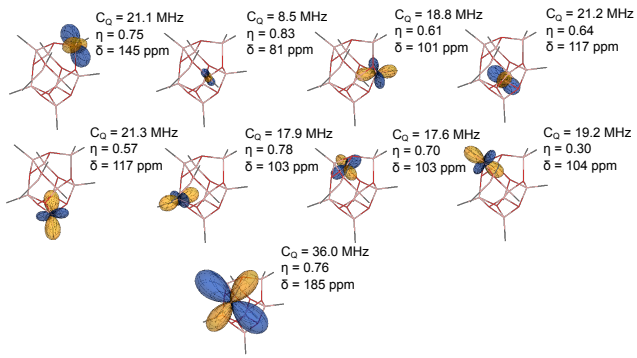

FIG. S23. ssnmr spectra of **(alome)$_{8,c}$ · (alme$_3$)$_2$**, simulated at different field strengths (the corresponding proton resonance frequencies are also provided).

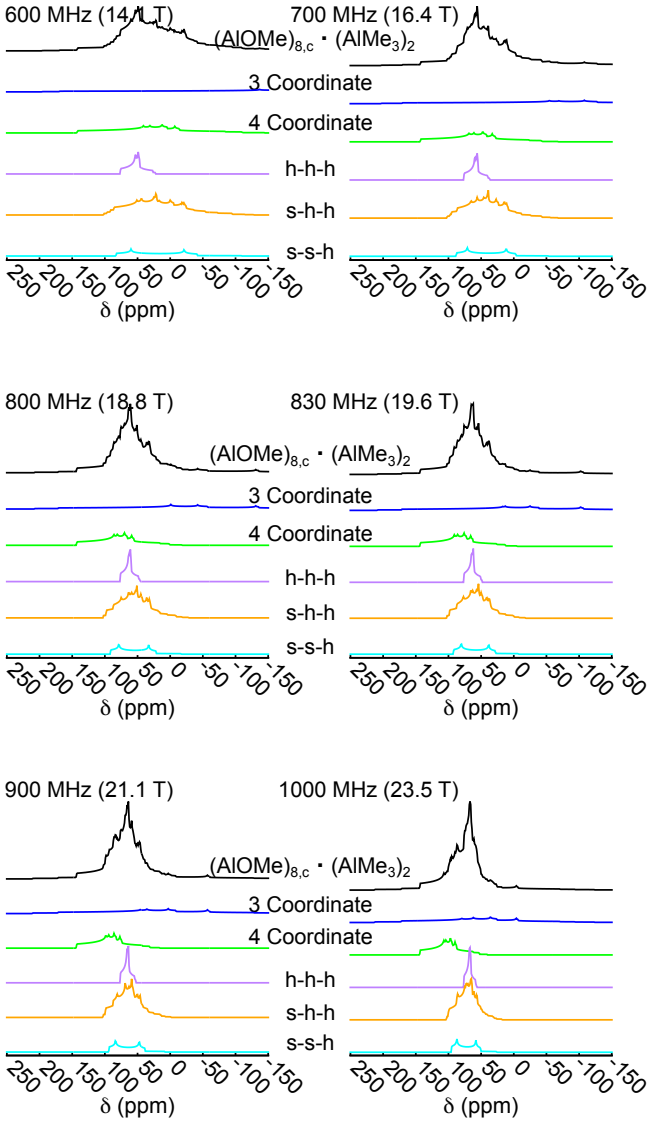

FIG. S24. Calculated EFG parameters and NMR chemical shifts of **(AlOMe)$_{8,c}$ · (AlMe$_3$)$_2$**.

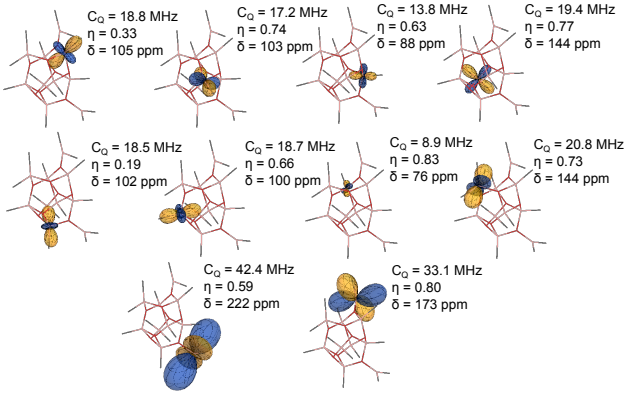

FIG. S25. SSNMR spectra of $\mathbf{(AlOMe)_{8,c} \cdot (AlMe_3)_3}$, simulated at different field strengths (the corresponding proton resonance frequencies are also provided).

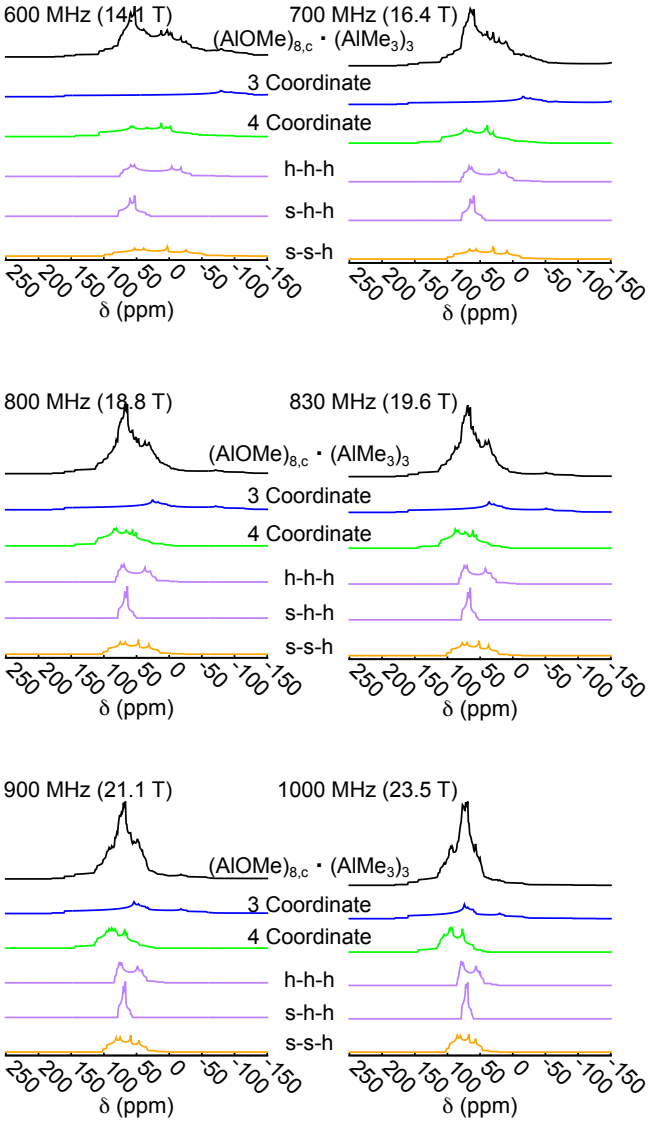

FIG. S26. Calculated EFG parameters and NMR chemical shifts of $\mathbf{(AlOMe)_{8,c} \cdot (AlMe_3)_3}$.

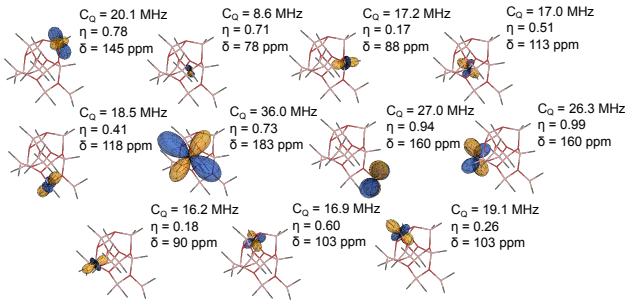

FIG. S27. SSNMR spectra of $\mathbf{(AlOMe)_{8,c} \cdot (AlMe_3)_4}$, simulated at different field strengths (the corresponding proton resonance frequencies are also provided).

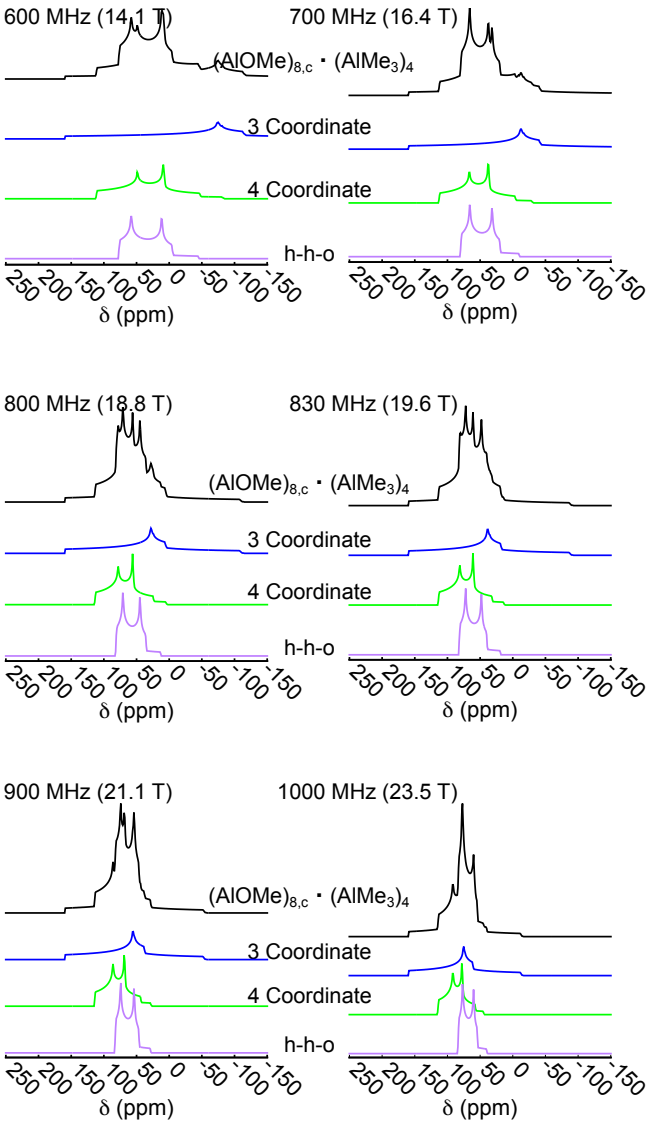

FIG. S28. Calculated EFG parameters and NMR chemical shifts of $\mathbf{(AlOMe)_{8,c} \cdot (AlMe_3)_4}$.

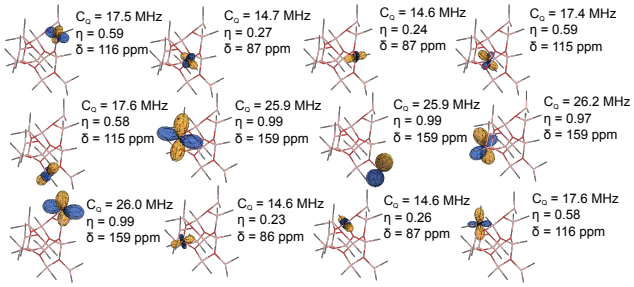

FIG. S29. SSNMR spectra of **(AlOMe)$_{10,c}$**, simulated at different field strengths (the corresponding proton resonance frequencies are also provided).

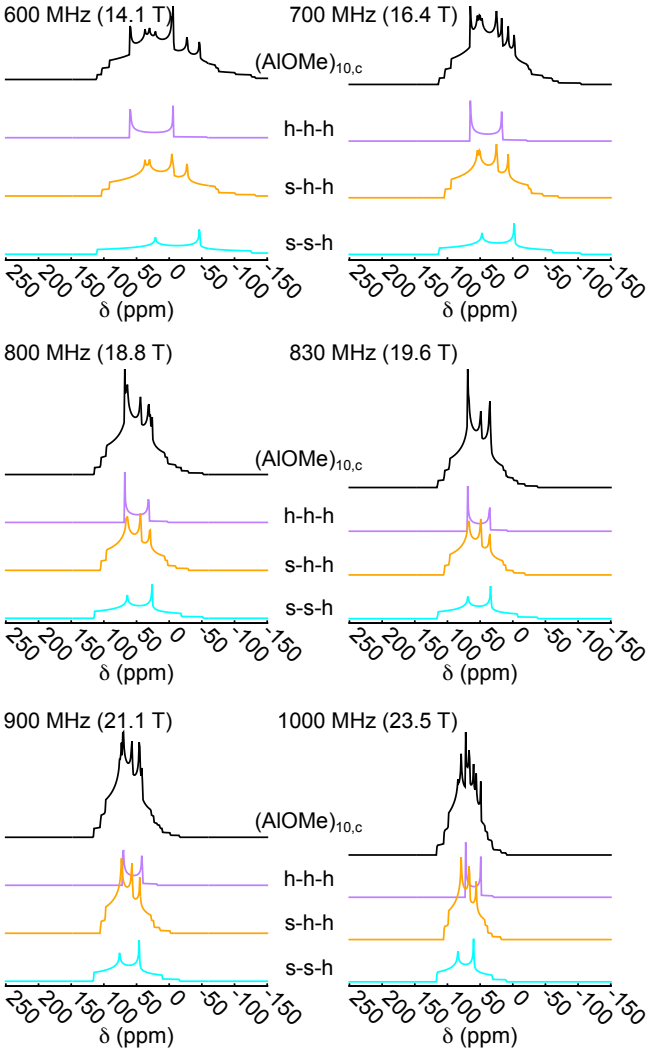

FIG. S30. Calculated EFG parameters and NMR chemical shifts of **(AlOMe)$_{10,c}$**.

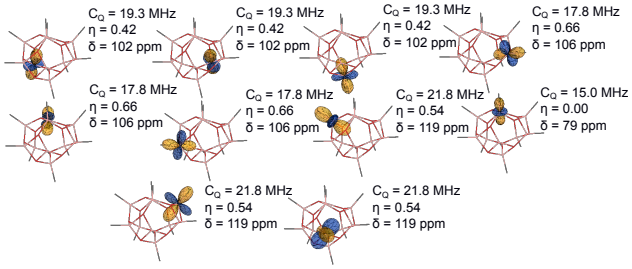

FIG. S31. SSNMR spectra of **(AlOMe)$_{10,c}$ · (AlMe$_3$)**, simulated at different field strengths (the corresponding proton resonance frequencies are also provided).

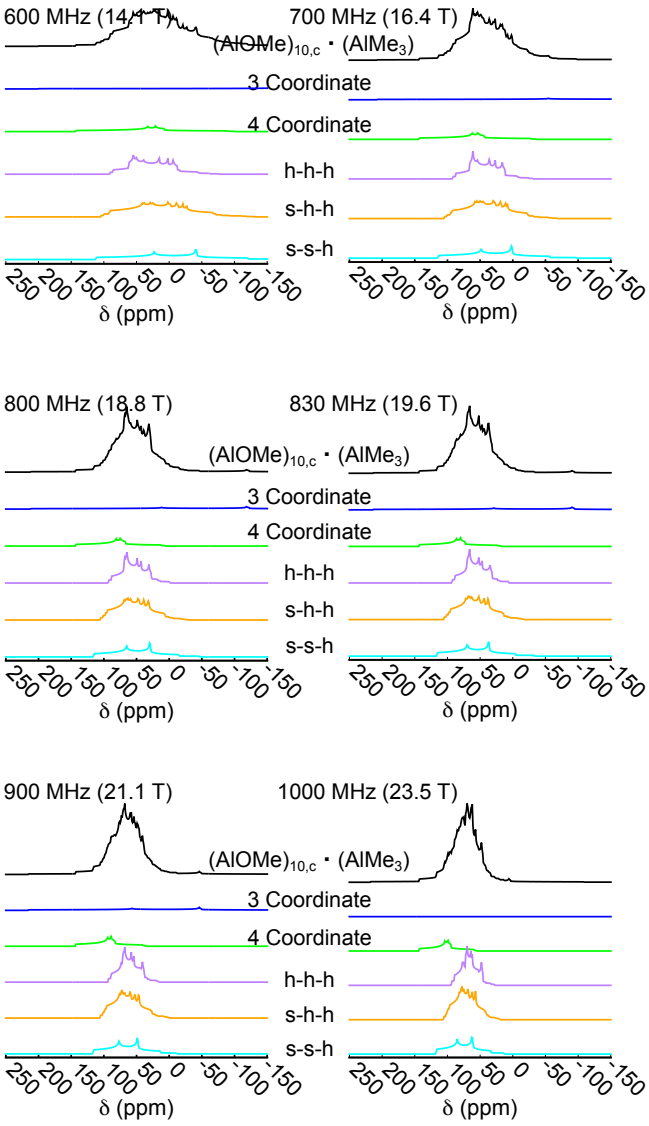

FIG. S32. Calculated EFG parameters and NMR chemical shifts of **(AlOMe)$_{10,c}$ · (AlMe$_3$)**.

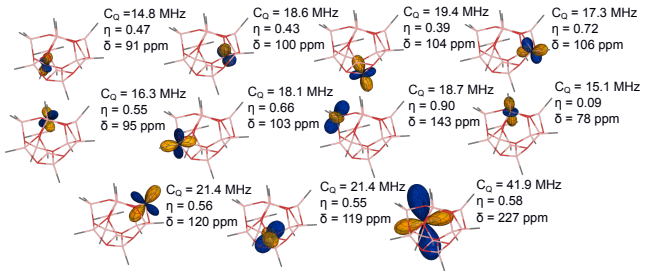

FIG. S33. SSNMR spectra of $\mathbf{(AlOMe)_{10,c} \cdot (AlMe_3)_2}$, simulated at different field strengths (the corresponding proton resonance frequencies are also provided).

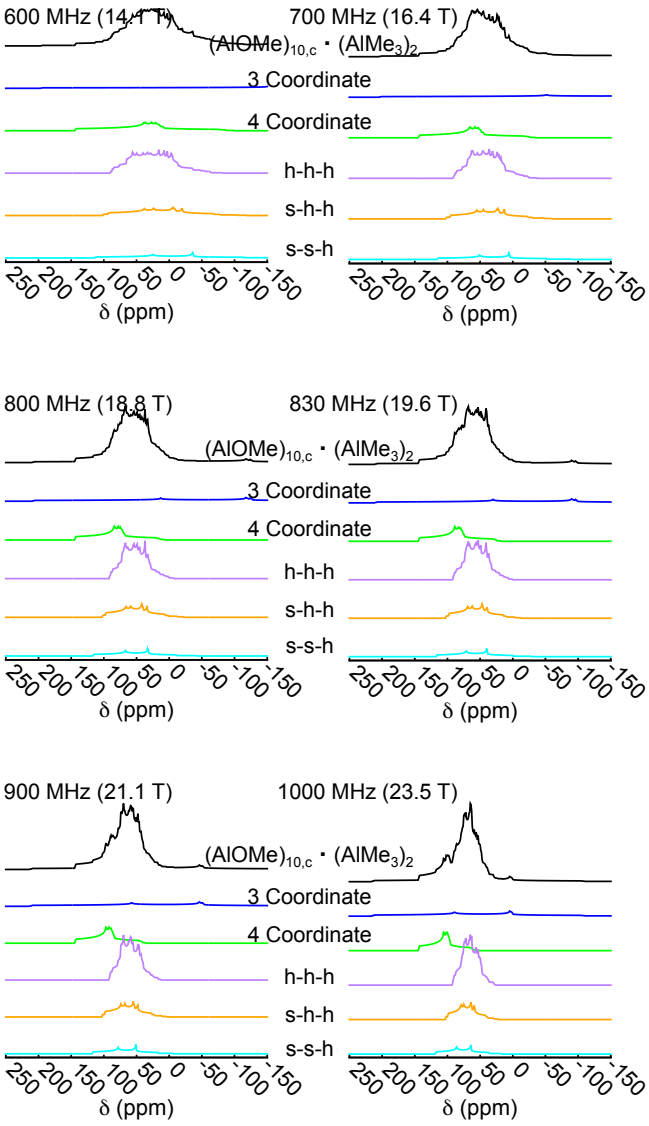

FIG. S34. Calculated EFG parameters and NMR chemical shifts of $\mathbf{(AlOMe)_{10,c} \cdot (AlMe_3)_2}$.

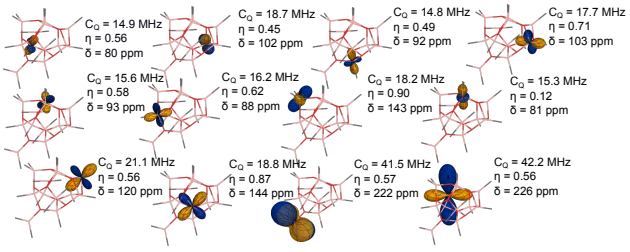

FIG. S35. SSNMR spectra of $\mathbf{(AlOMe)_{10,c} \cdot (AlMe_3)_3}$, simulated at different field strengths (the corresponding proton resonance frequencies are also provided).

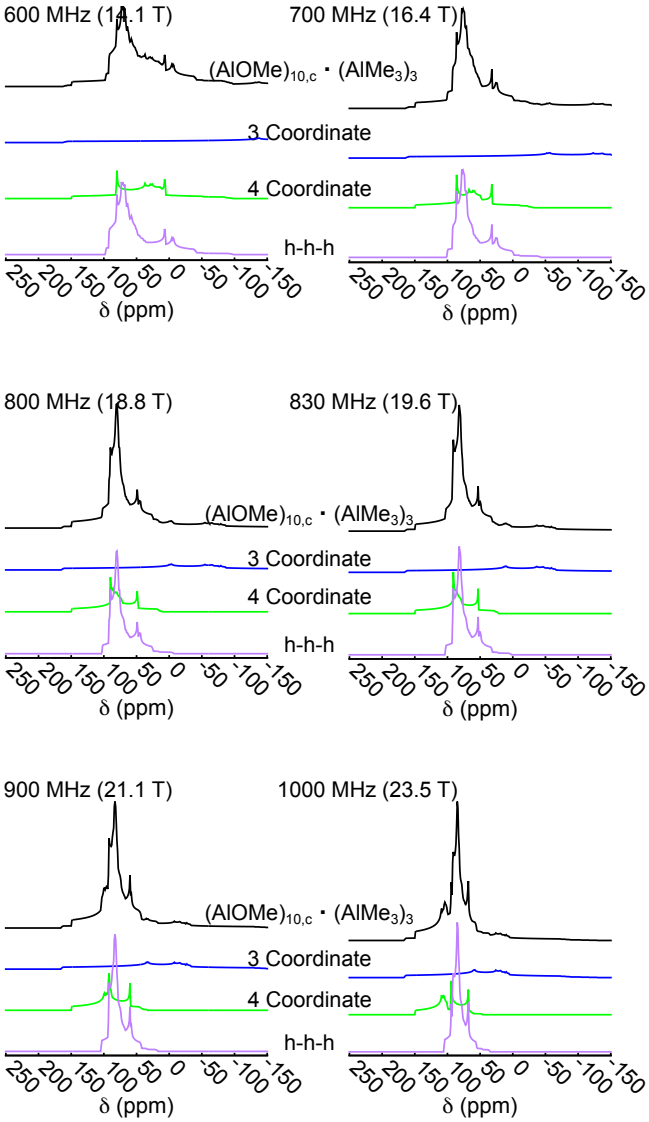

FIG. S36. Calculated EFG parameters and NMR chemical shifts of $\mathbf{(AlOMe)_{10,c} \cdot (AlMe_3)_3}$.

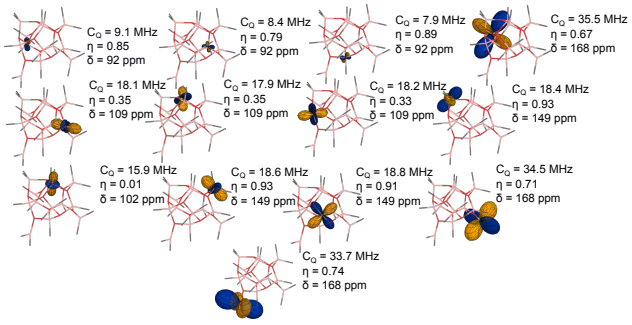

FIG. S37. SSNMR spectra of **(AlOMe)$_{12,c}$**, simulated at different field strengths (the corresponding proton resonance frequencies are also provided).

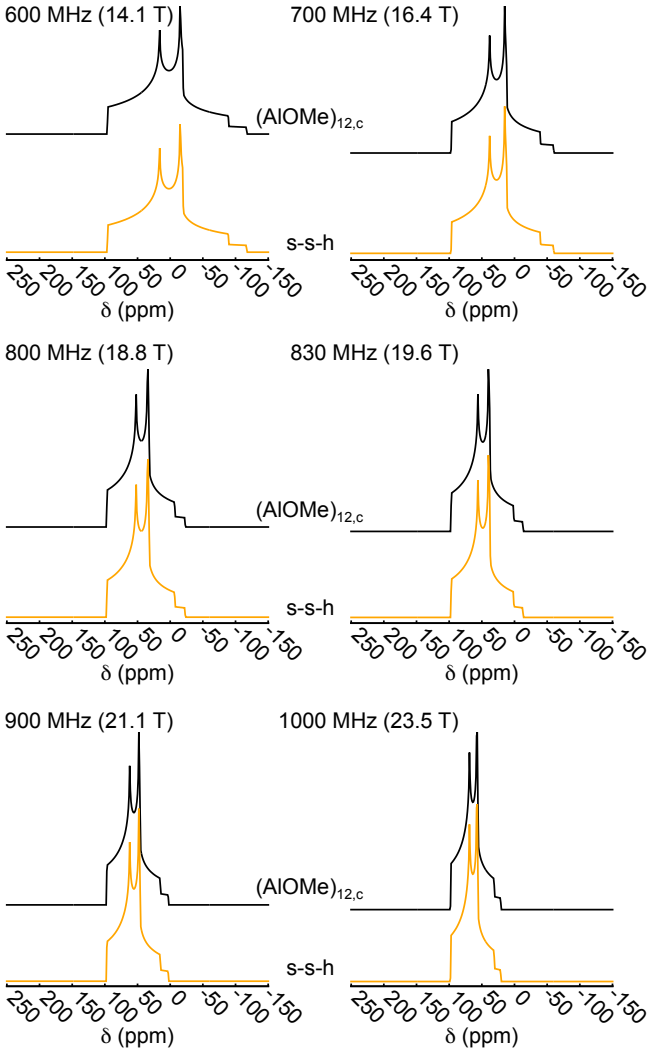

FIG. S38. Calculated EFG parameters and NMR chemical shifts of **(AlOMe)$_{12,c}$**.

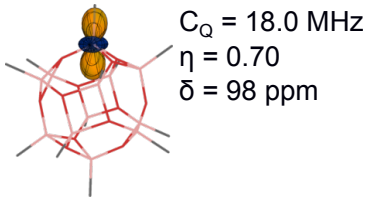

FIG. S39. SSNMR spectra of **(AlOMe)$_{14,c}$**, simulated at different field strengths (the corresponding proton resonance frequencies are also provided).

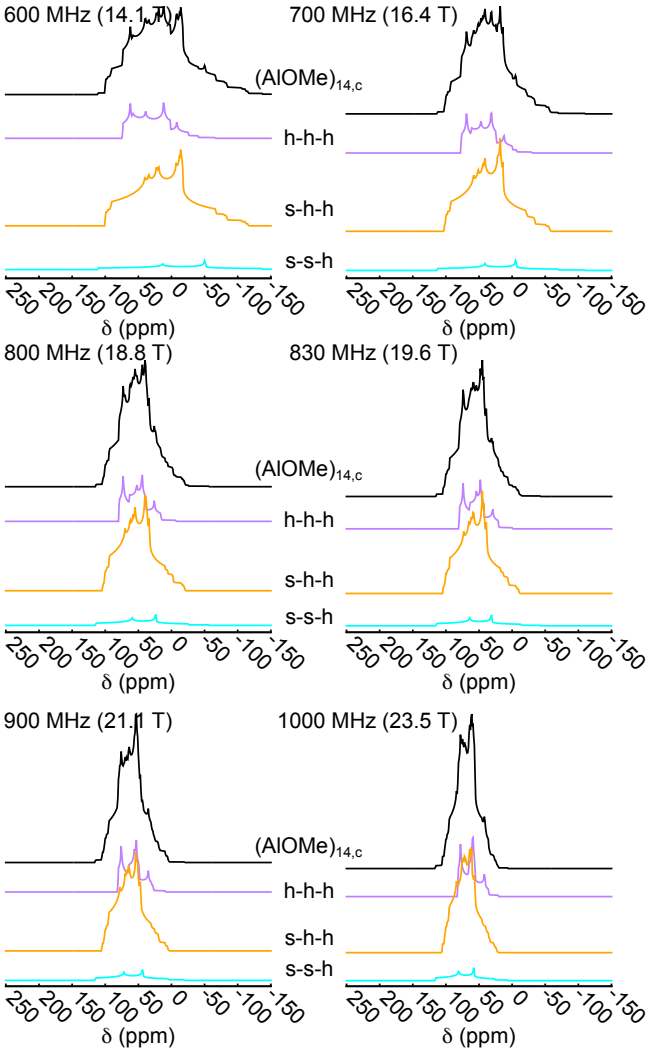

FIG. S40. Calculated EFG parameters and NMR chemical shifts of **(AlOMe)$_{14,c}$**.

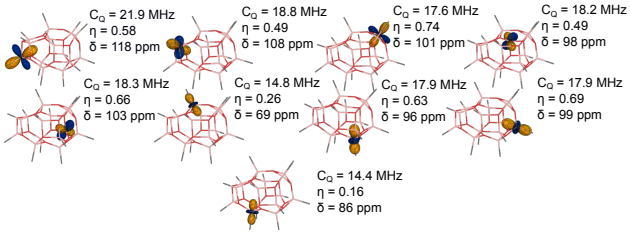

FIG. S41. SSNMR spectra of **(AlOMe)$_{14,c}$ · (AlMe$_3$)**, simulated at different field strengths (the corresponding proton resonance frequencies are also provided).

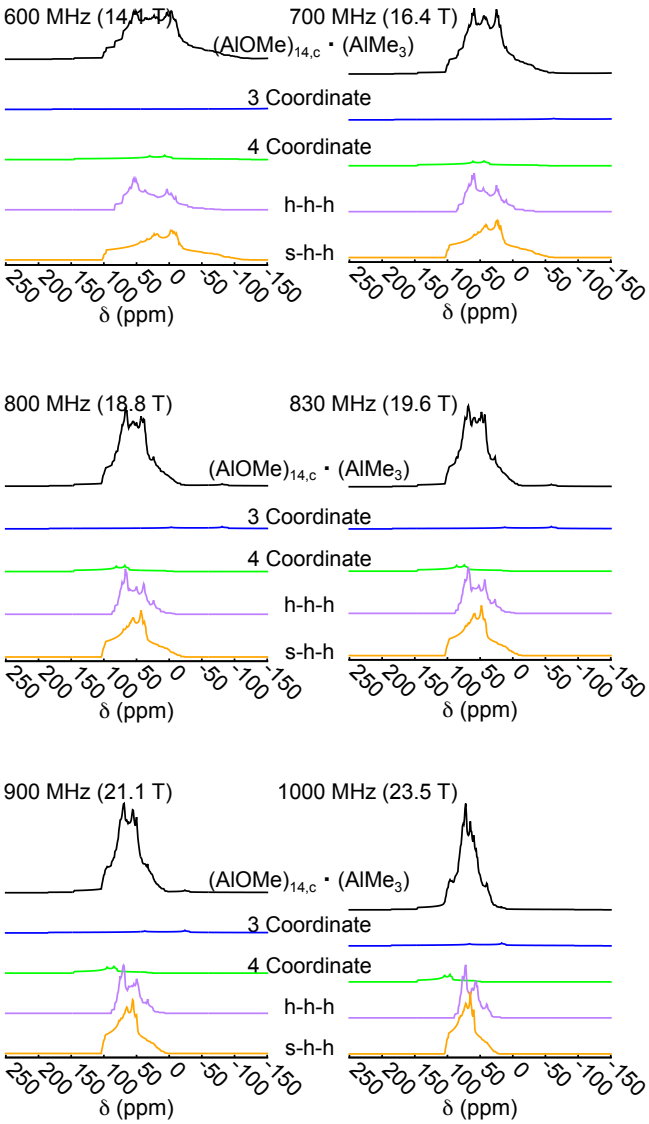

FIG. S42. Calculated EFG parameters and NMR chemical shifts of **(AlOMe)$_{14,c}$ · (AlMe$_3$)**.

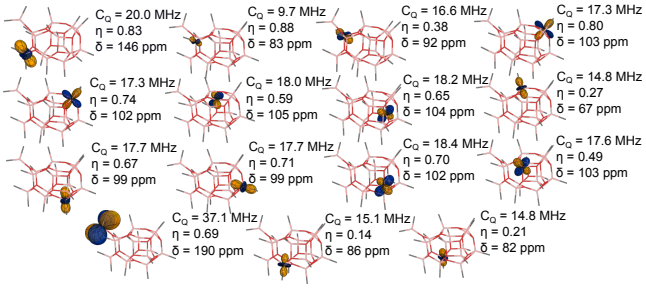

FIG. S43. SSNMR spectra of **(AlOMe)$_{16,c}$**, simulated at different field strengths (the corresponding proton resonance frequencies are also provided).

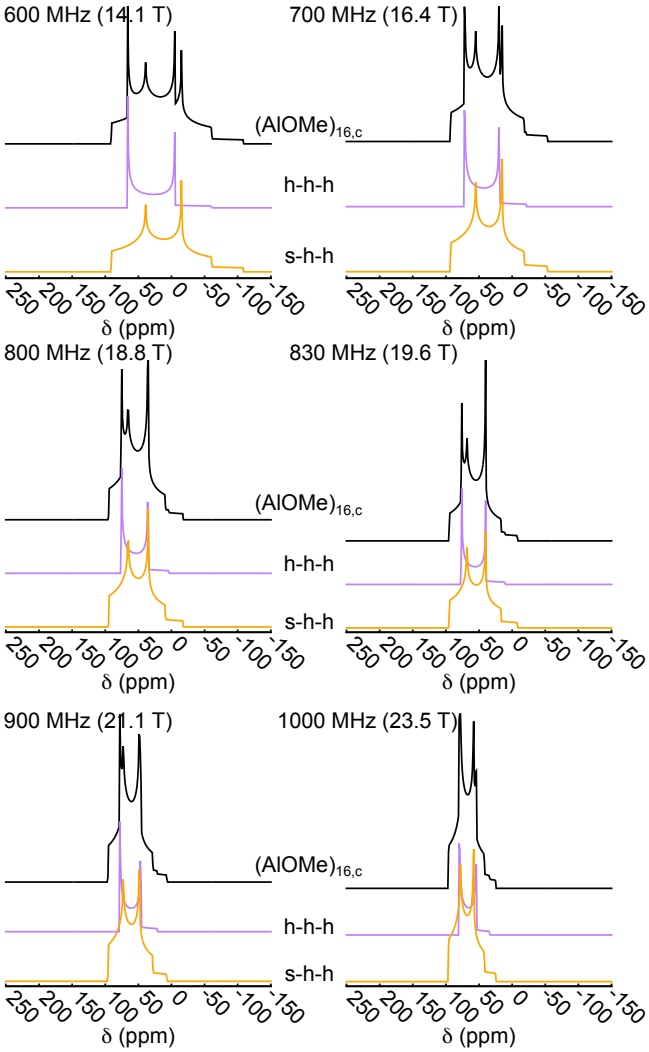

FIG. S44. Calculated EFG parameters and NMR chemical shifts of **(AlOMe)$_{16,c}$**.

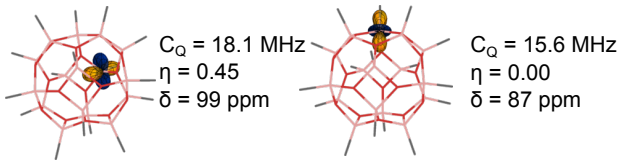

FIG. S45. SSNMR spectra of **(AlOMe)$_{18,c}$**, simulated at different field strengths (the corresponding proton resonance frequencies are also provided).

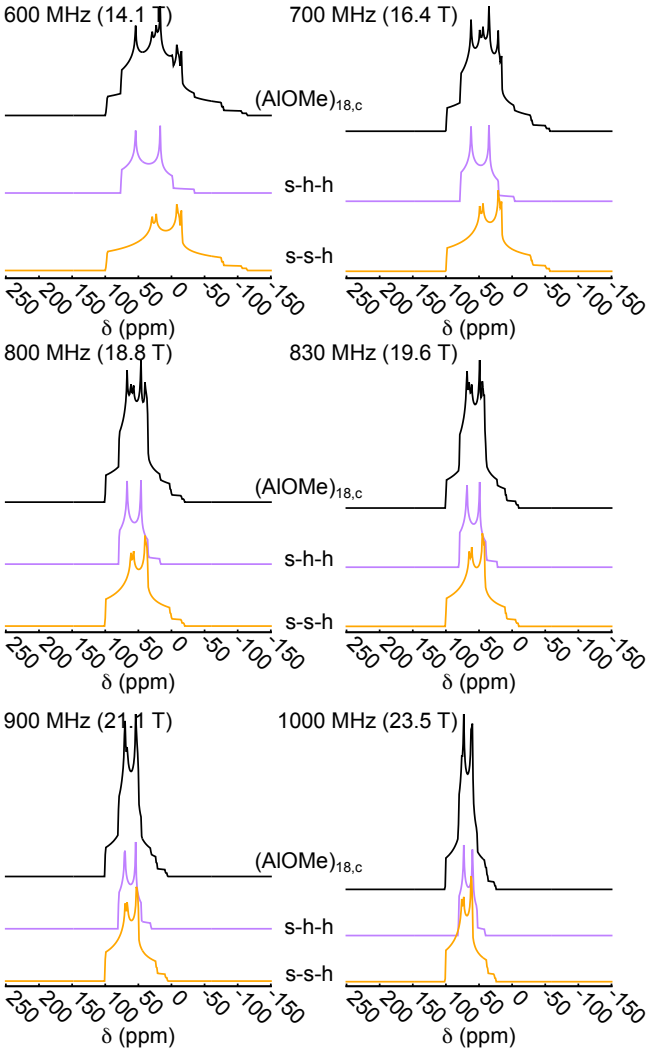

FIG. S46. Calculated EFG parameters and NMR chemical shifts of **(AlOMe)$_{18,c}$**.

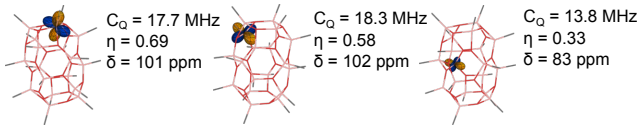

FIG. S47. SSNMR spectra of **(AlOMe)$_{20,c}$**, simulated at different field strengths (the corresponding proton resonance frequencies are also provided).

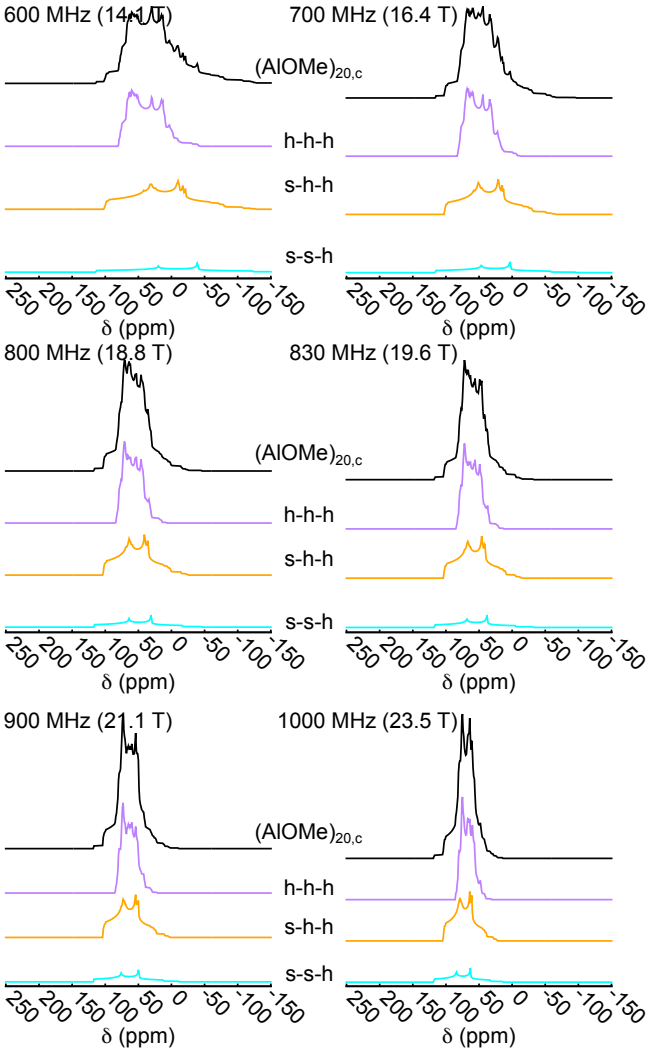

FIG. S48. Calculated EFG parameters and NMR chemical shifts of **(AlOMe)$_{20,c}$**.

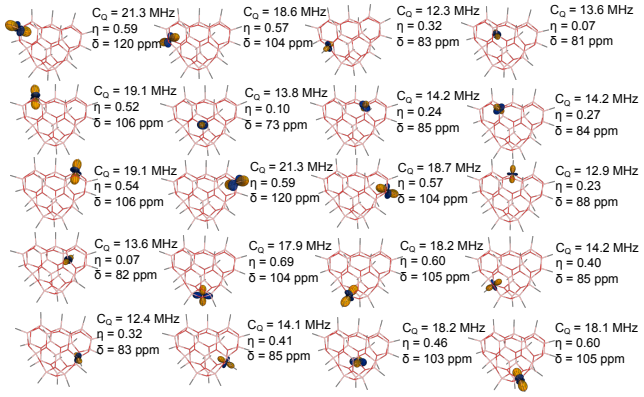

FIG. S49. SSNMR spectra of **$(AlOMe)_{20,c} \cdot (AlMe_3)$**, simulated at different field strengths (the corresponding proton resonance frequencies are also provided).

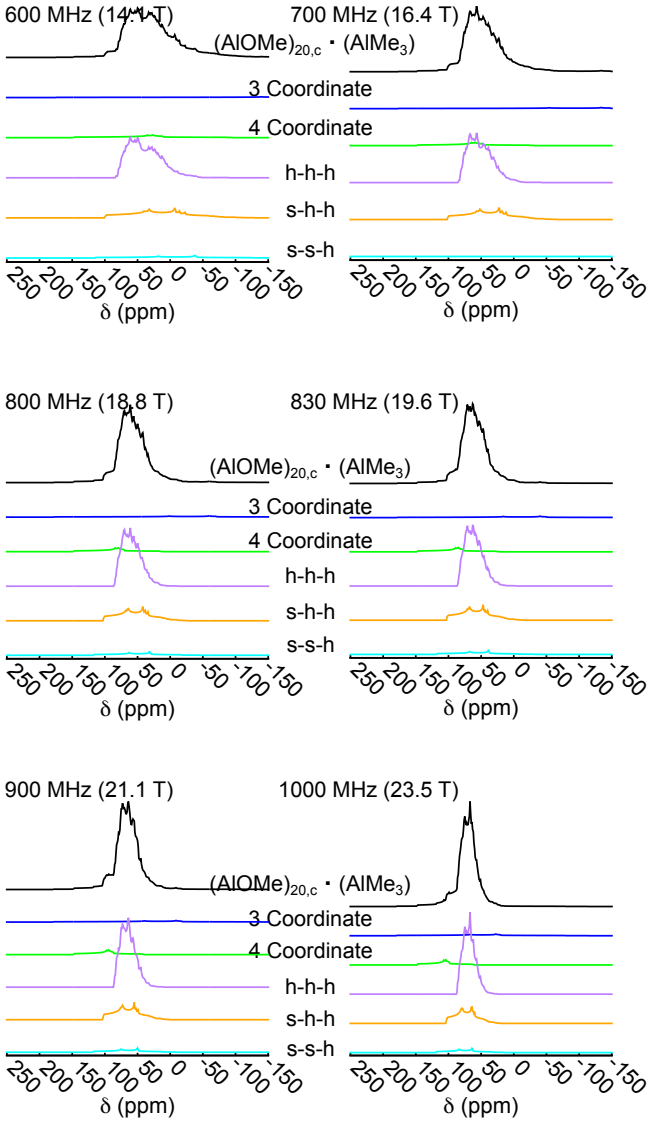

FIG. S50. Calculated EFG parameters and NMR chemical shifts of $\mathbf{(AlOMe)_{20,c} \cdot (AlMe_3)}$.

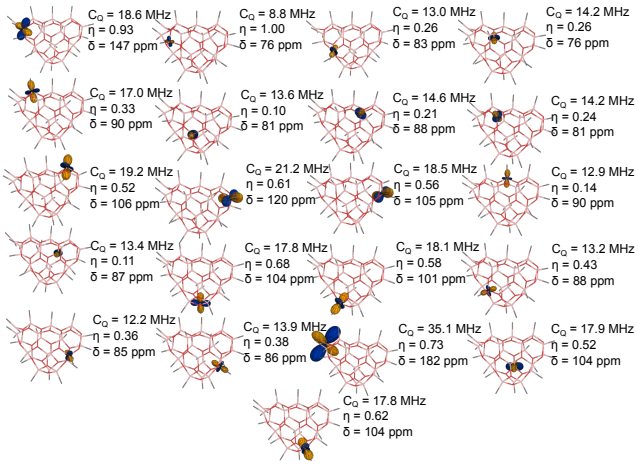

FIG. S51. SSNMR spectra of **$(AlOMe)_{20,c} \cdot (AlMe_3)_2$**, simulated at different field strengths (the corresponding proton resonance frequencies are also provided).

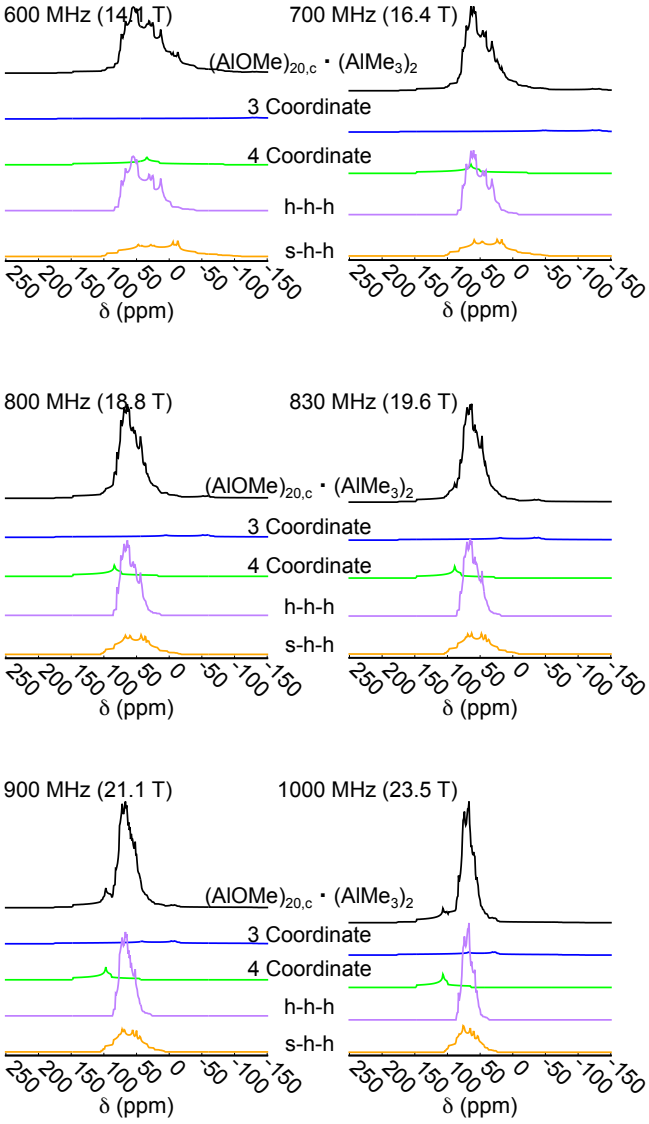

FIG. S52. Calculated EFG parameters and NMR chemical shifts of $\mathbf{(AlOMe)_{20,c} \cdot (AlMe_3)_2}$.

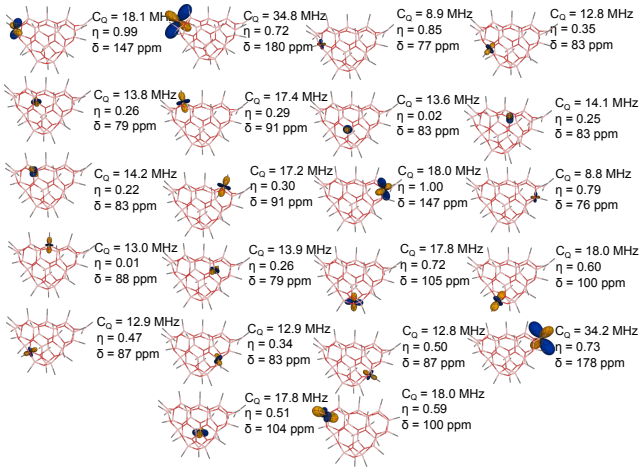

FIG. S53. SSNMR spectra of **(AlOMe)$_{10,t}$**, simulated at different field strengths (the corresponding proton resonance frequencies are also provided).

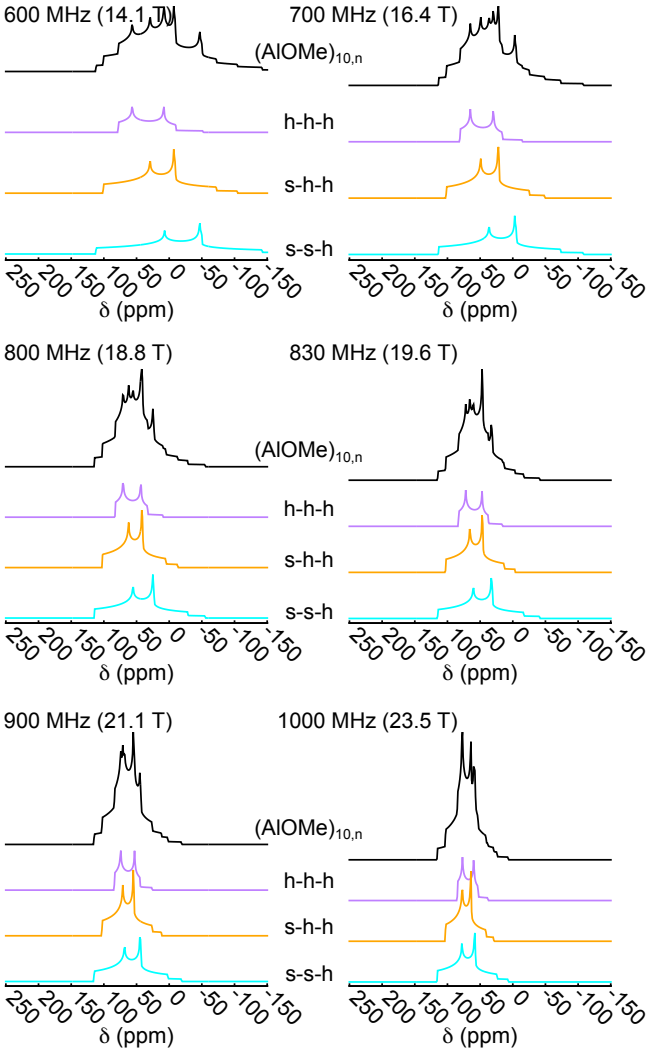

FIG. S54. Calculated EFG parameters and NMR chemical shifts of **(AlOMe)$_{10,t}$**.

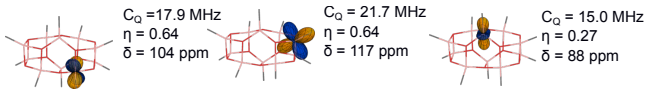

FIG. S55. SSNMR spectra of **(AlOMe)$_{10,t}$ · (AlMe$_3$)**, simulated at different field strengths (the corresponding proton resonance frequencies are also provided).

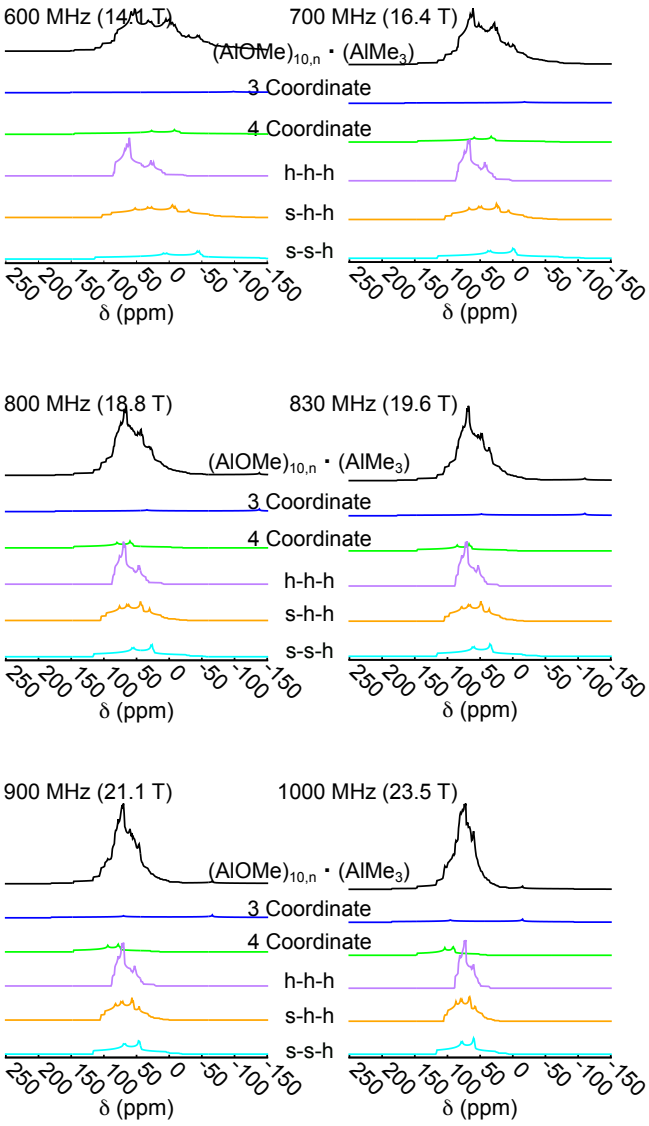

FIG. S56. Calculated EFG parameters and NMR chemical shifts of **(AlOMe)$_{10,t}$ · (AlMe$_3$)**.

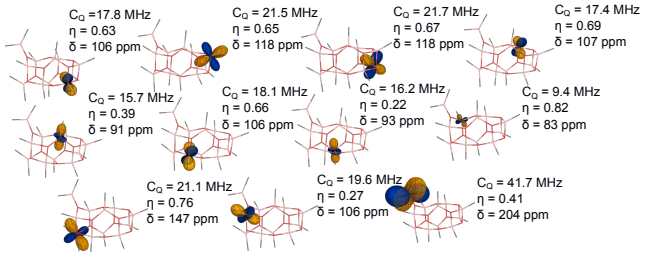

FIG. S57. SSNMR spectra of **(AlOMe)$_{10,t}$ · (AlMe$_3$)$_2$**, simulated at different field strengths (the corresponding proton resonance frequencies are also provided).

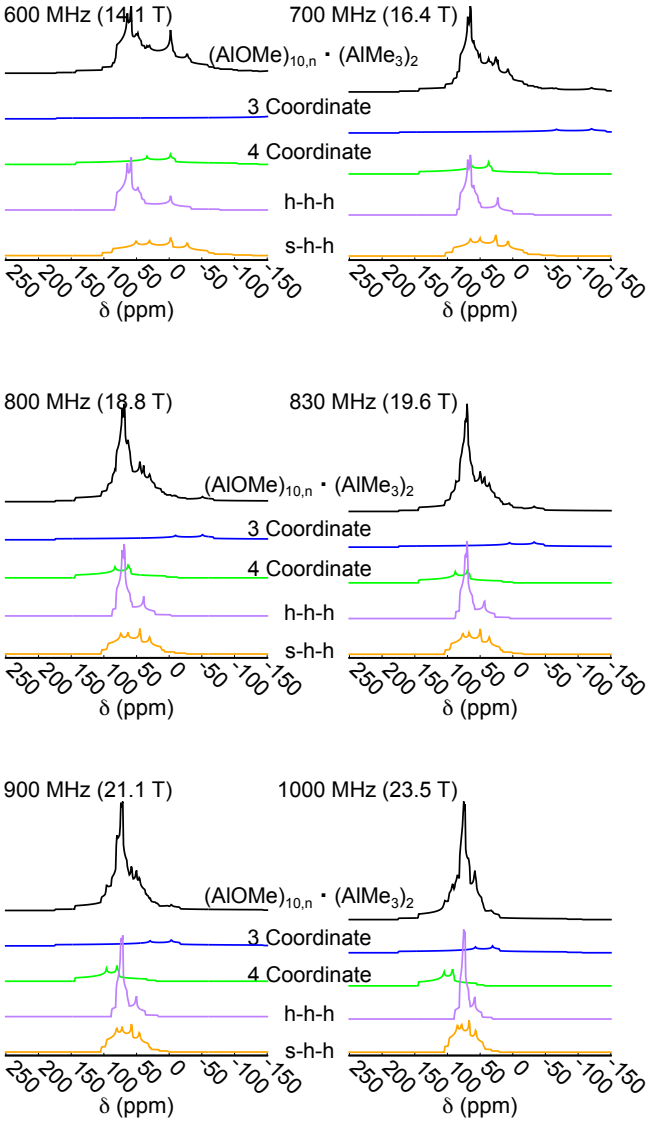

FIG. S58. Calculated EFG parameters and NMR chemical shifts of **(AlOMe)$_{10,t}$ · (AlMe$_3$)$_2$**.

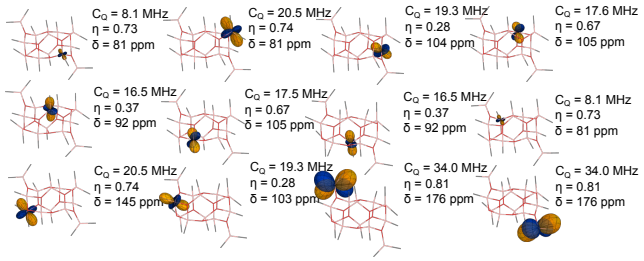

FIG. S59. SSNMR spectra of **(AlOMe)$_{10,t}$ · (AlMe$_3$)$_3$**, simulated at different field strengths (the corresponding proton resonance frequencies are also provided).

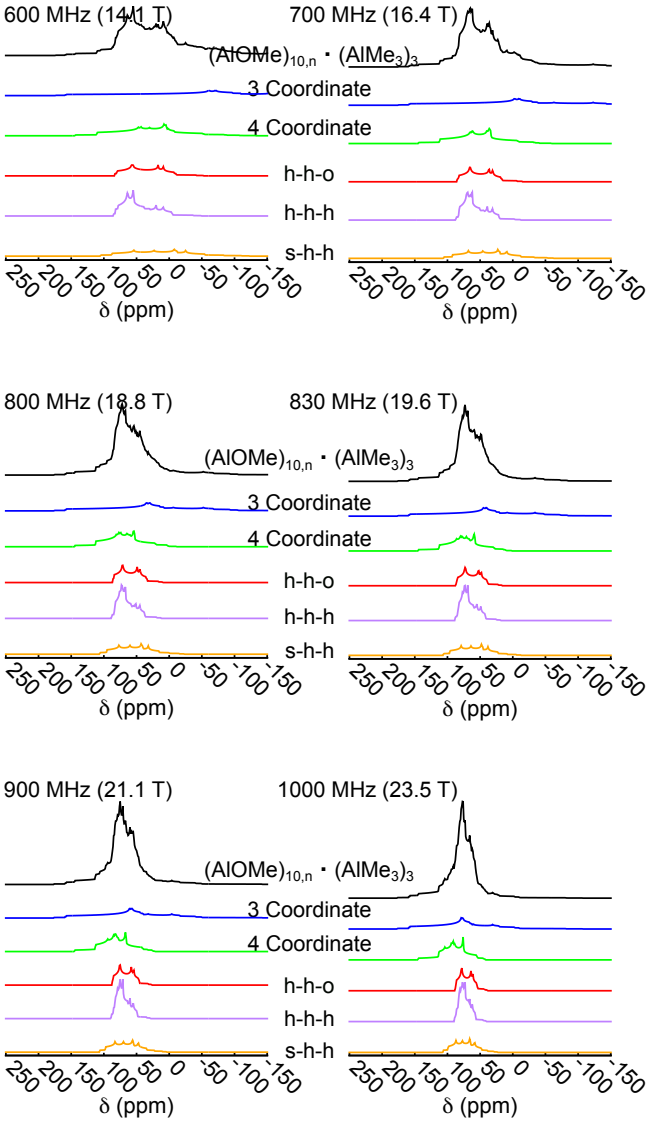

FIG. S60. Calculated EFG parameters and NMR chemical shifts of **(AlOMe)$_{10,t}$ · (AlMe$_3$)$_3$**.

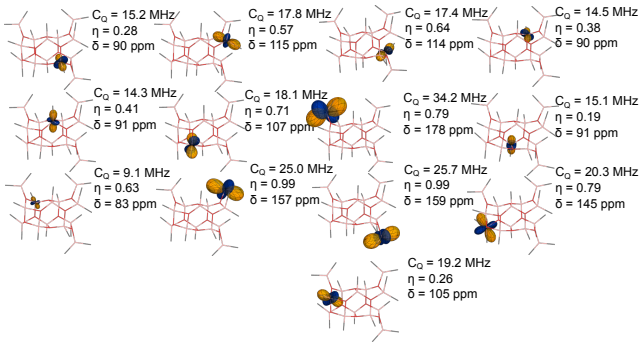

FIG. S61. SSNMR spectra of **(AlOMe)$_{10,t}$ · (AlMe$_3$)$_4$**, simulated at different field strengths (the corresponding proton resonance frequencies are also provided).

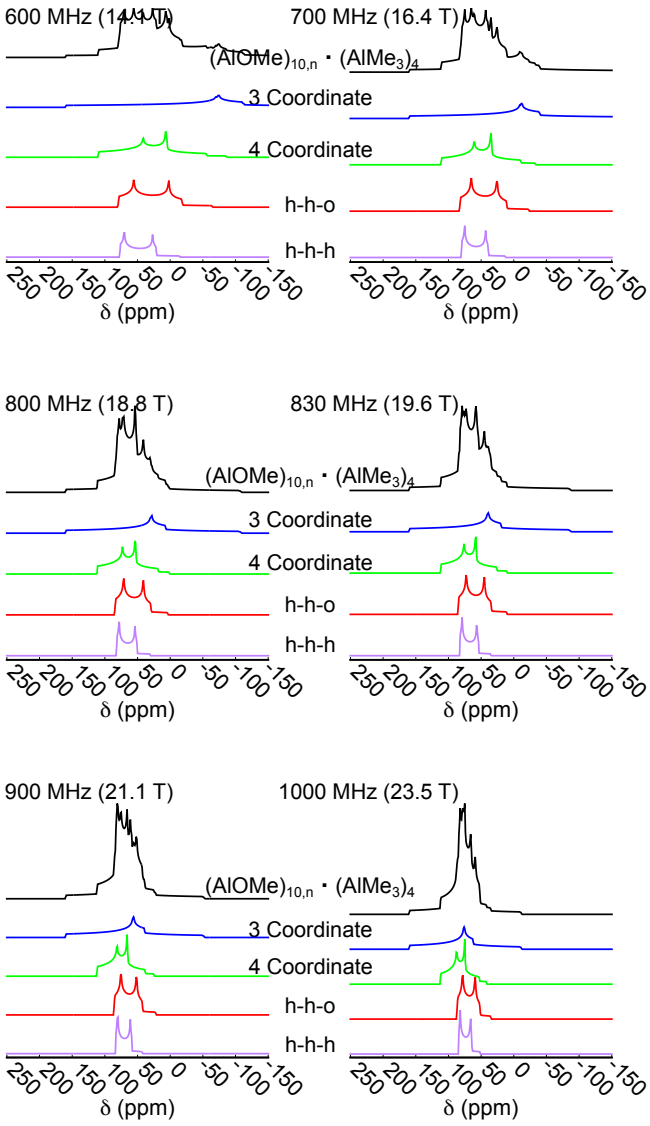

FIG. S62. Calculated EFG parameters and NMR chemical shifts of **(AlOMe)$_{10,t}$ · (AlMe$_3$)$_4$**.

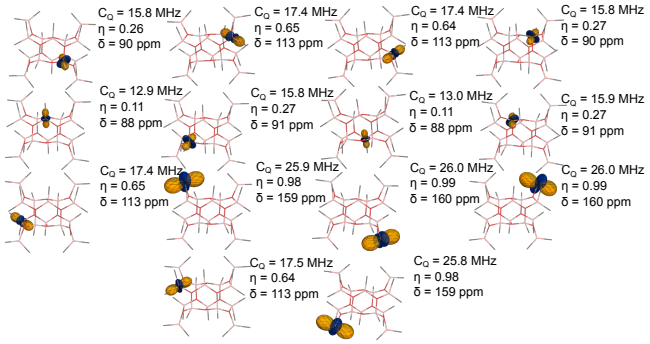

FIG. S63. SSNMR spectra of **(AlOMe)$_{12,t}$**, simulated at different field strengths (the corresponding proton resonance frequencies are also provided).

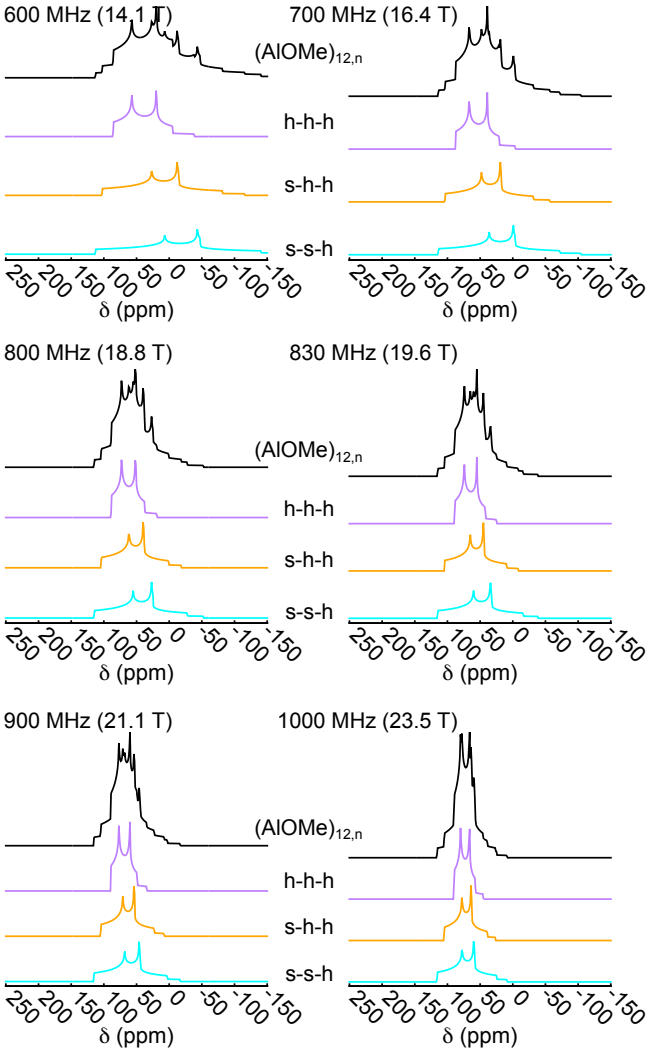

FIG. S64. Calculated EFG parameters and NMR chemical shifts of **(AlOMe)$_{12,t}$**.

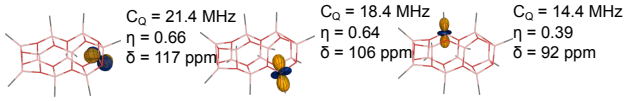

FIG. S65. SSNMR spectra of **(AlOMe)$_{12,t}$ · (AlMe$_3$)**, simulated at different field strengths (the corresponding proton resonance frequencies are also provided).

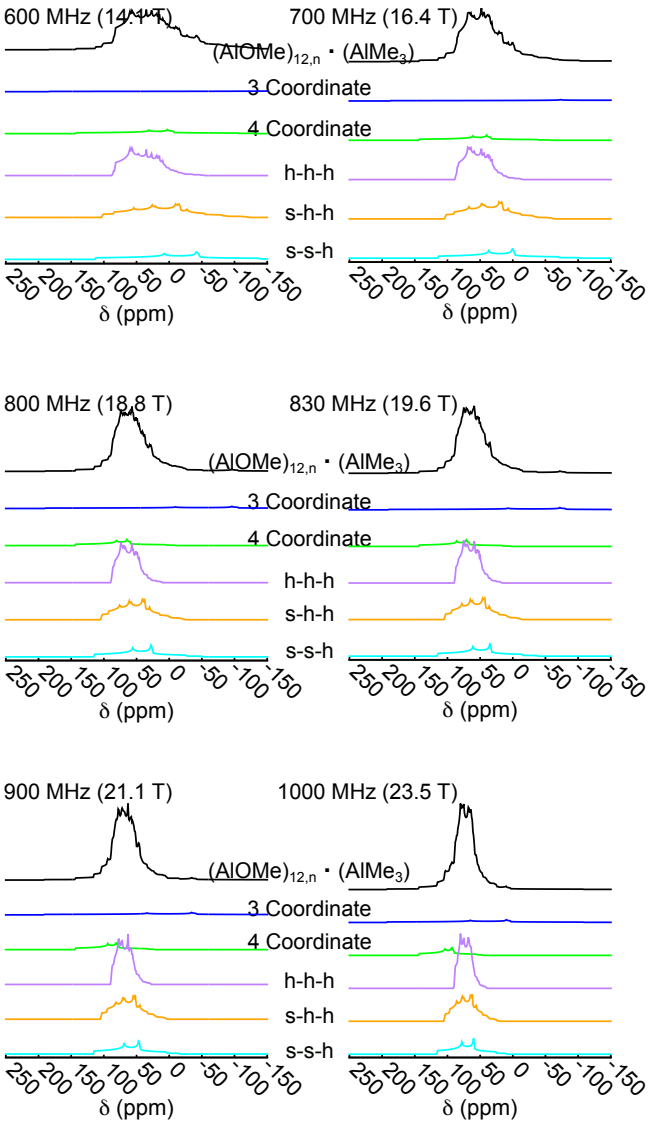

FIG. S66. Calculated EFG parameters and NMR chemical shifts of **(AlOMe)$_{12,t}$ · (AlMe$_3$)**.

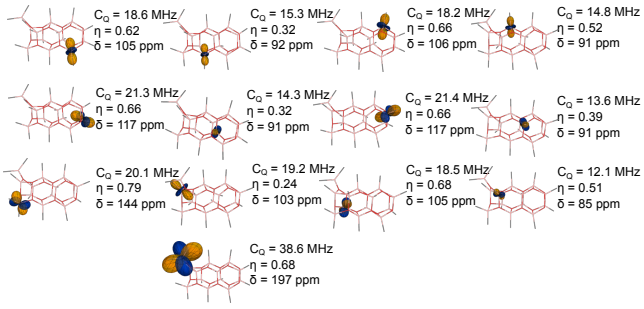

FIG. S67. SSNMR spectra of **(AlOMe)$_{12,t}$ · (AlMe$_3$)$_2$**, simulated at different field strengths (the corresponding proton resonance frequencies are also provided).

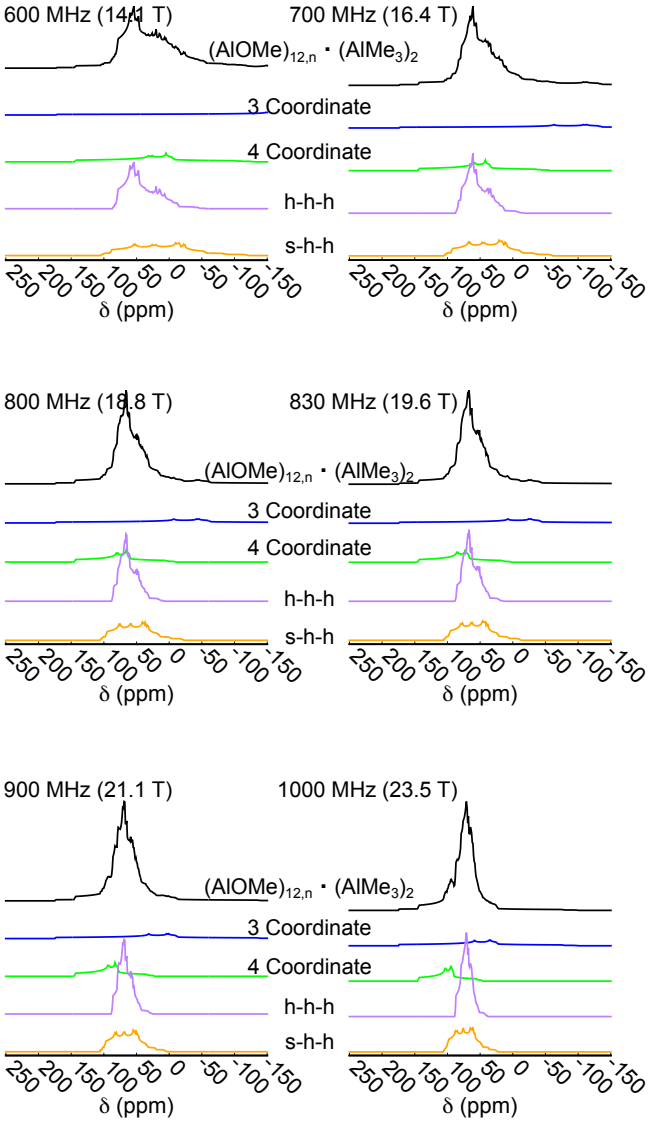

FIG. S68. Calculated EFG parameters and NMR chemical shifts of **(AlOMe)$_{12,t}$ · (AlMe$_3$)$_2$**.

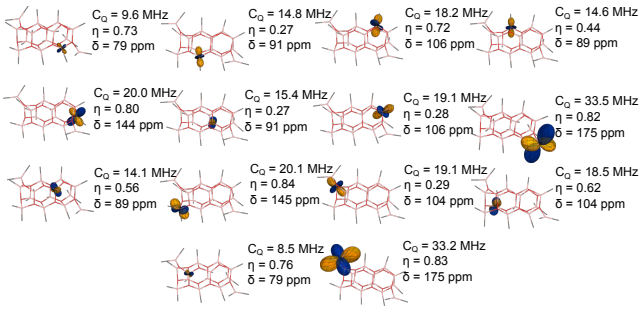

FIG. S69. SSNMR spectra of **(AlOMe)$_{12,t}$ · (AlMe$_3$)$_3$**, simulated at different field strengths (the corresponding proton resonance frequencies are also provided).

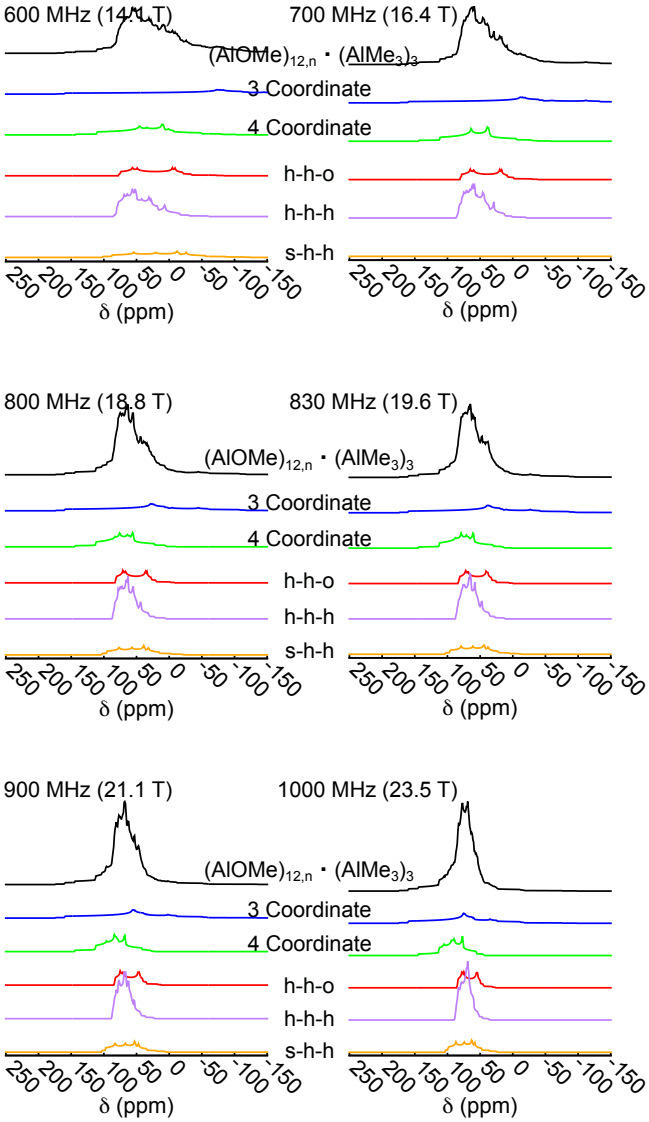

FIG. S70. Calculated EFG parameters and NMR chemical shifts of **(AlOMe)$_{12,t}$ · (AlMe$_3$)$_3$**.

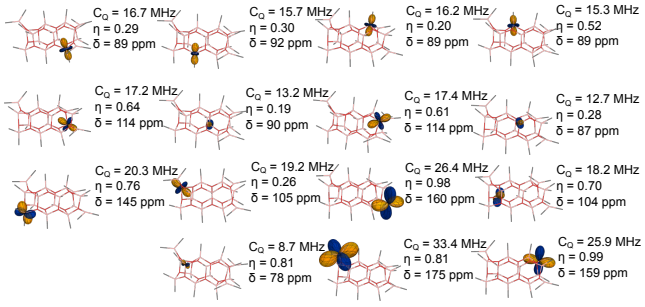

FIG. S71. SSNMR spectra of **(AlOMe)$_{12,t}$ · (AlMe$_3$)$_4$**, simulated at different field strengths (the corresponding proton resonance frequencies are also provided).

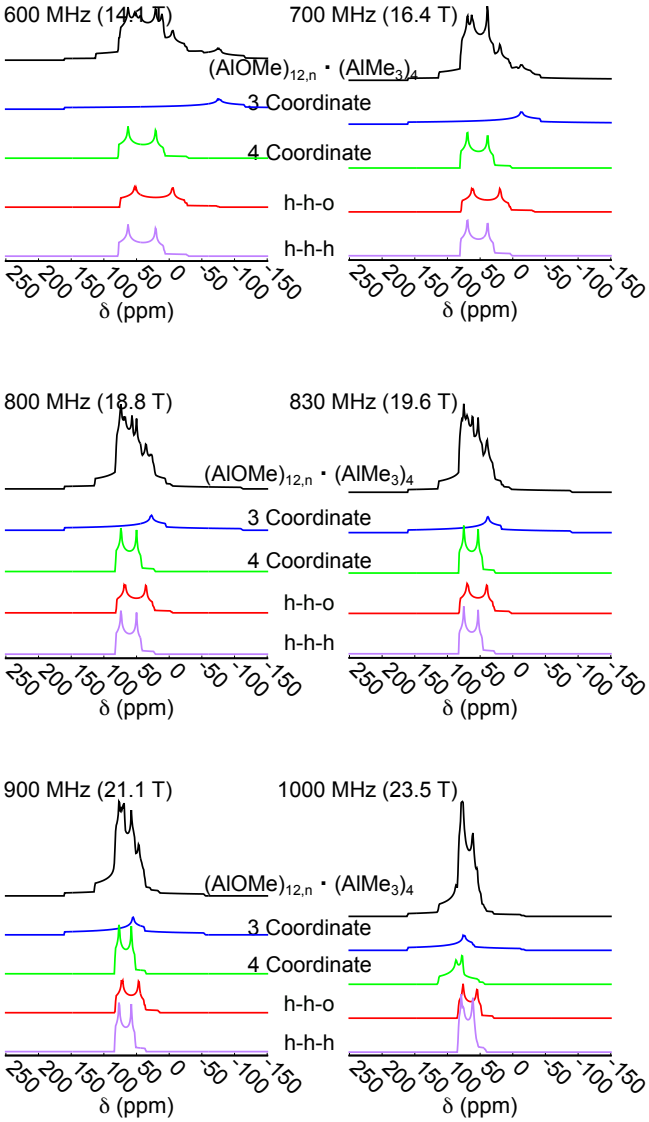

FIG. S72. Calculated EFG parameters and NMR chemical shifts of **(AlOMe)$_{12,t}$ · (AlMe$_3$)$_4$**.

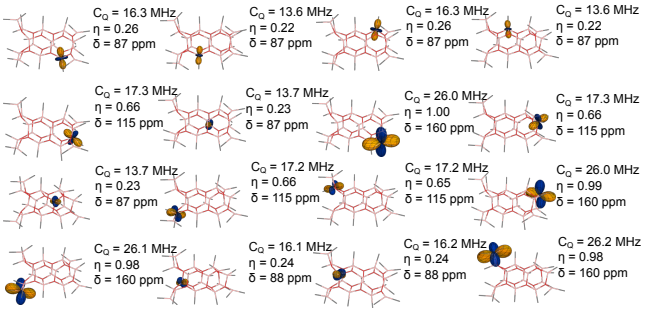

FIG. S73. SSNMR spectra of **(AlOMe)$_{14,t}$**, simulated at different field strengths (the corresponding proton resonance frequencies are also provided).

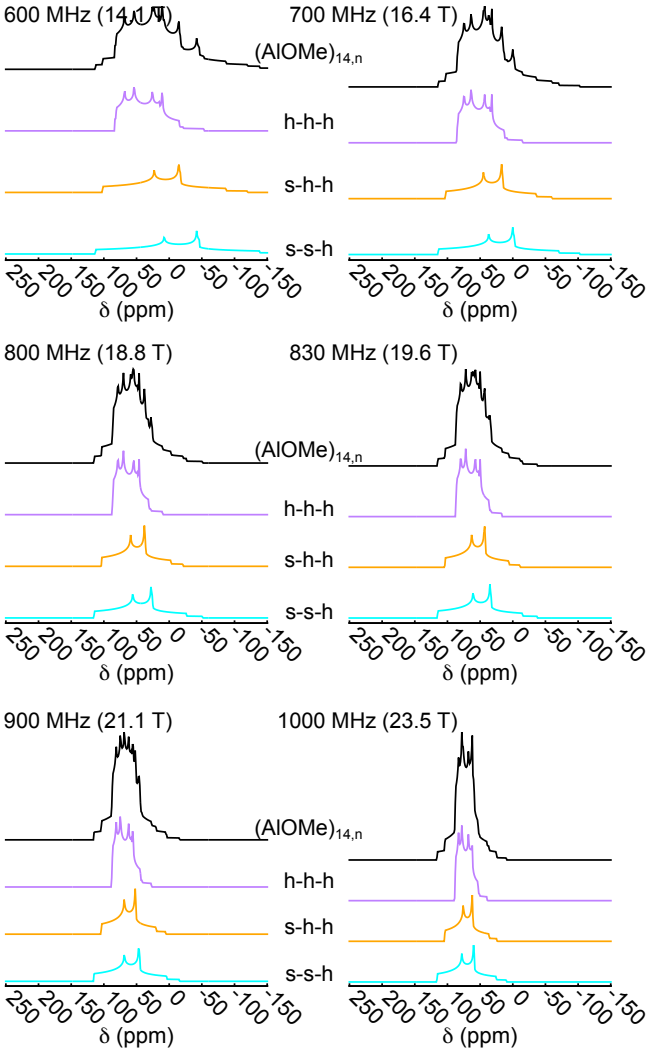

FIG. S74. Calculated EFG parameters and NMR chemical shifts of **(AlOMe)$_{14,t}$**.

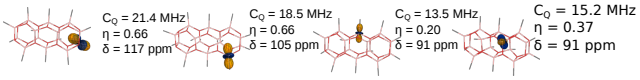

FIG. S75. SSNMR spectra of **(AlOMe)$_{14,t}$ · (AlMe$_3$)**, simulated at different field strengths (the corresponding proton resonance frequencies are also provided).

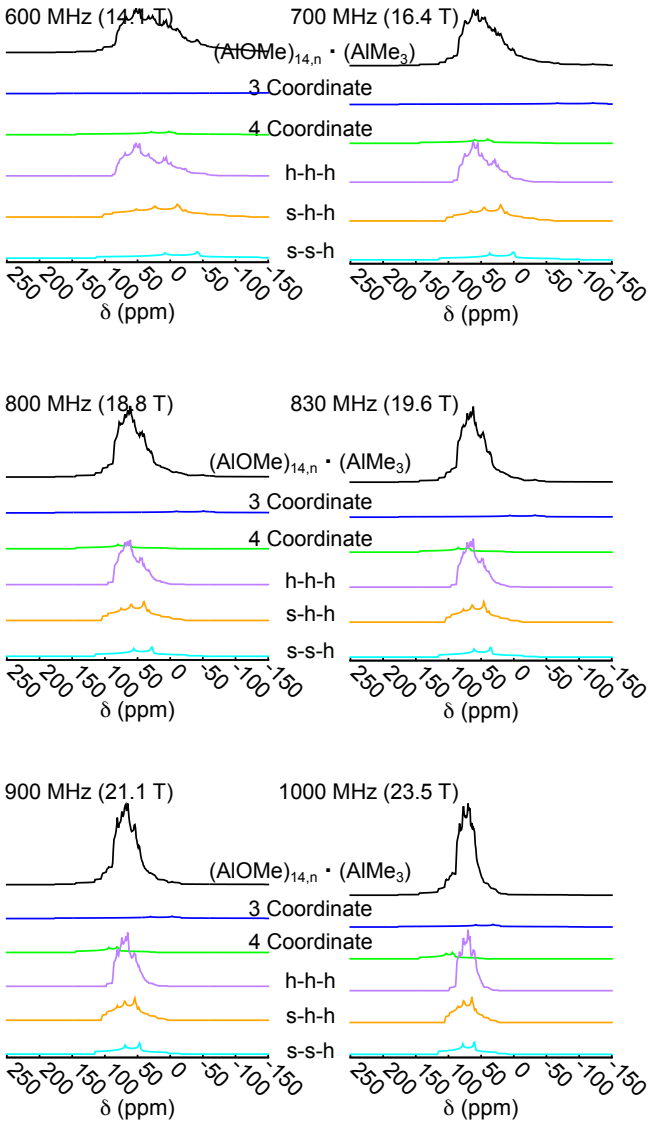

FIG. S76. Calculated EFG parameters and NMR chemical shifts of **(AlOMe)$_{14,t}$ · (AlMe$_3$)**.

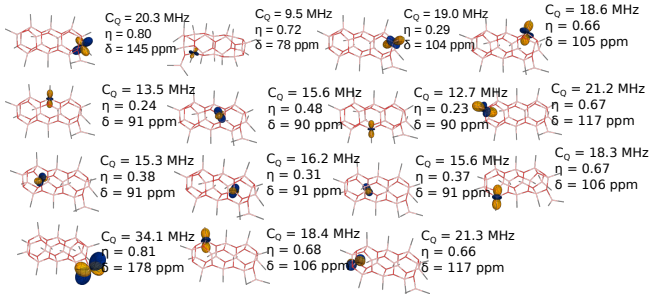

FIG. S77. SSNMR spectra of $\mathbf{(AlOMe)_{14,t} \cdot (AlMe_3)_2}$, simulated at different field strengths (the corresponding proton resonance frequencies are also provided).

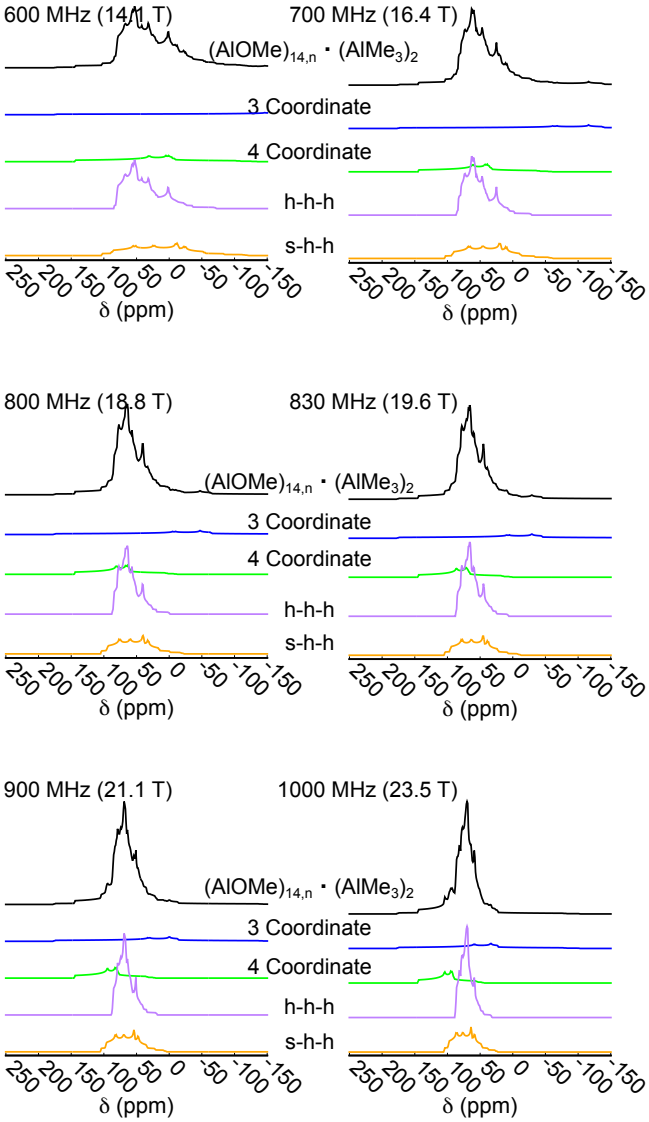

FIG. S78. Calculated EFG parameters and NMR chemical shifts of $\mathbf{(AlOMe)_{14,t} \cdot (AlMe_3)_2}$.

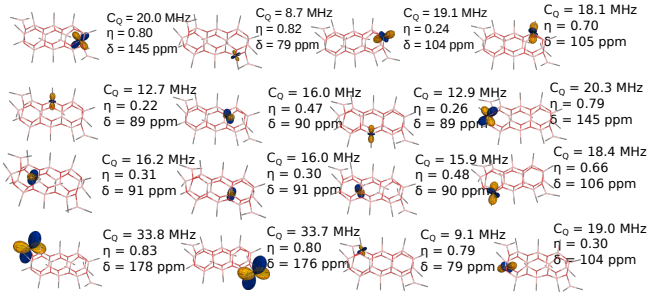

FIG. S79. SSNMR spectra of **(AlOMe)$_{14,t}$ · (AlMe$_3$)$_3$**, simulated at different field strengths (the corresponding proton resonance frequencies are also provided).

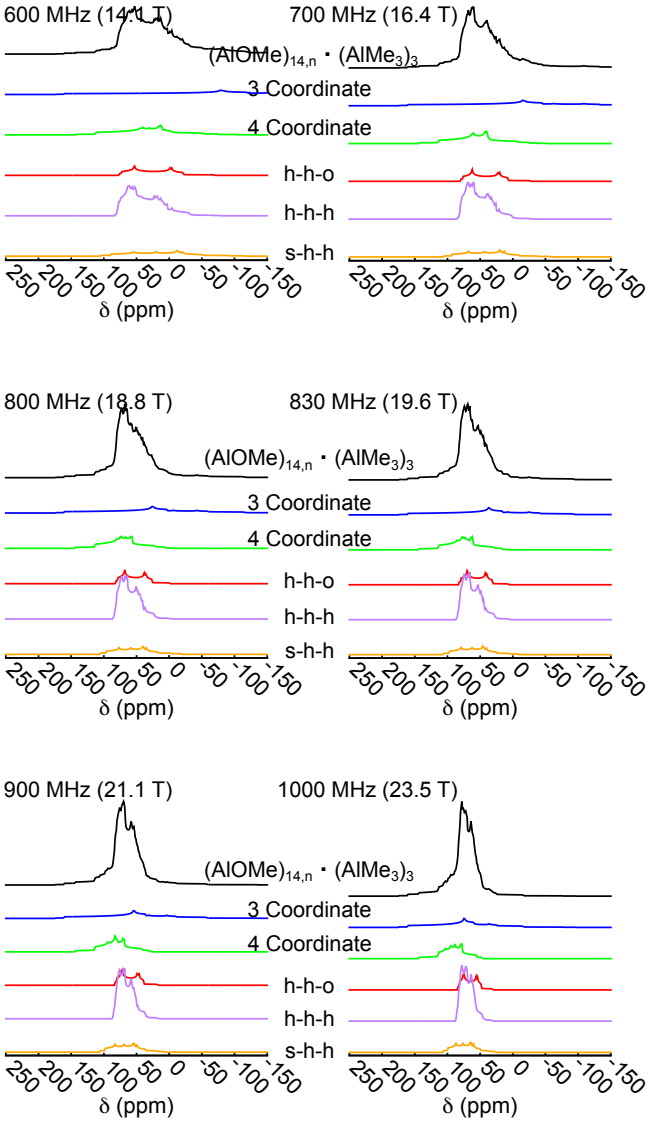

FIG. S80. Calculated EFG parameters and NMR chemical shifts of **(AlOMe)$_{14,t}$ · (AlMe$_3$)$_3$**.

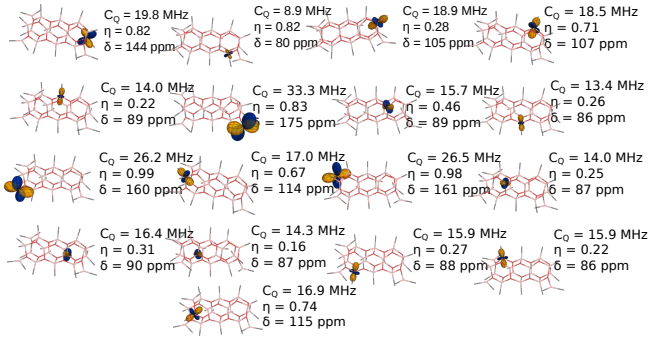

FIG. S81. SSNMR spectra of $\mathbf{(AlOMe)_{14,t} \cdot (AlMe_3)_4}$, simulated at different field strengths (the corresponding proton resonance frequencies are also provided).

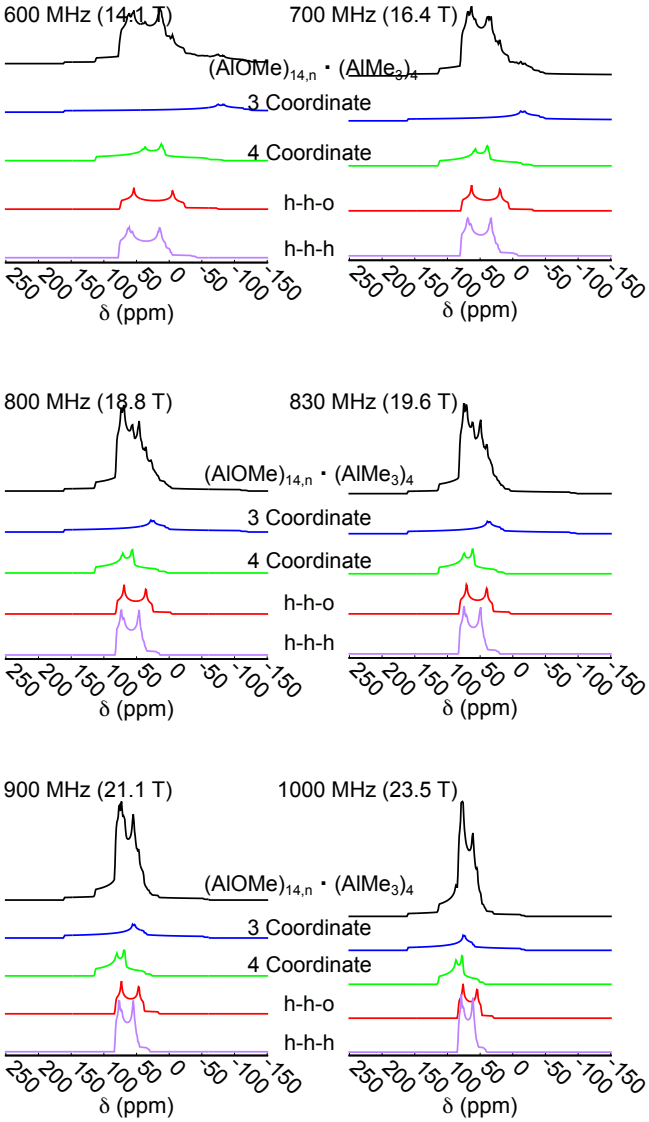

FIG. S82. Calculated EFG parameters and NMR chemical shifts of $\mathbf{(AlOMe)_{14,t} \cdot (AlMe_3)_4}$.

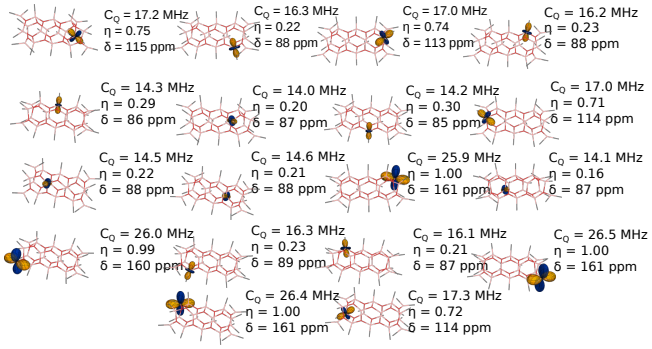

FIG. S83. SSNMR spectra of **(AlOMe)$_{16,t}$**, simulated at different field strengths (the corresponding proton resonance frequencies are also provided).

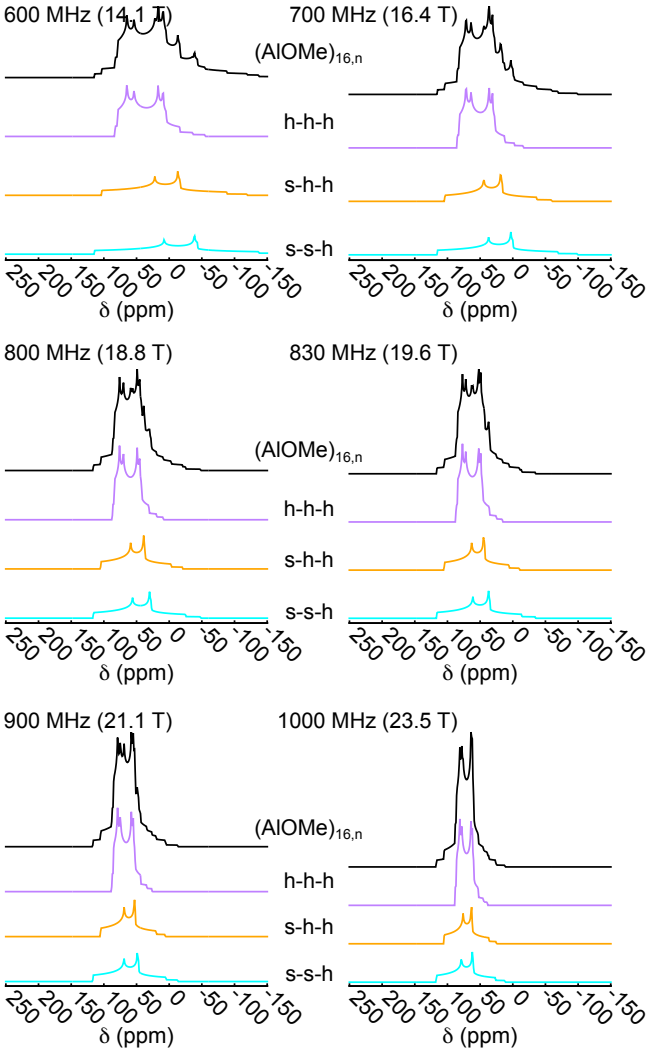

FIG. S84. Calculated EFG parameters and NMR chemical shifts of **(AlOMe)$_{16,t}$**.

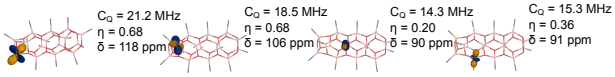

FIG. S85. SSNMR spectra of **(AlOMe)$_{16,t}$ · (AlMe$_3$)**, simulated at different field strengths (the corresponding proton resonance frequencies are also provided).

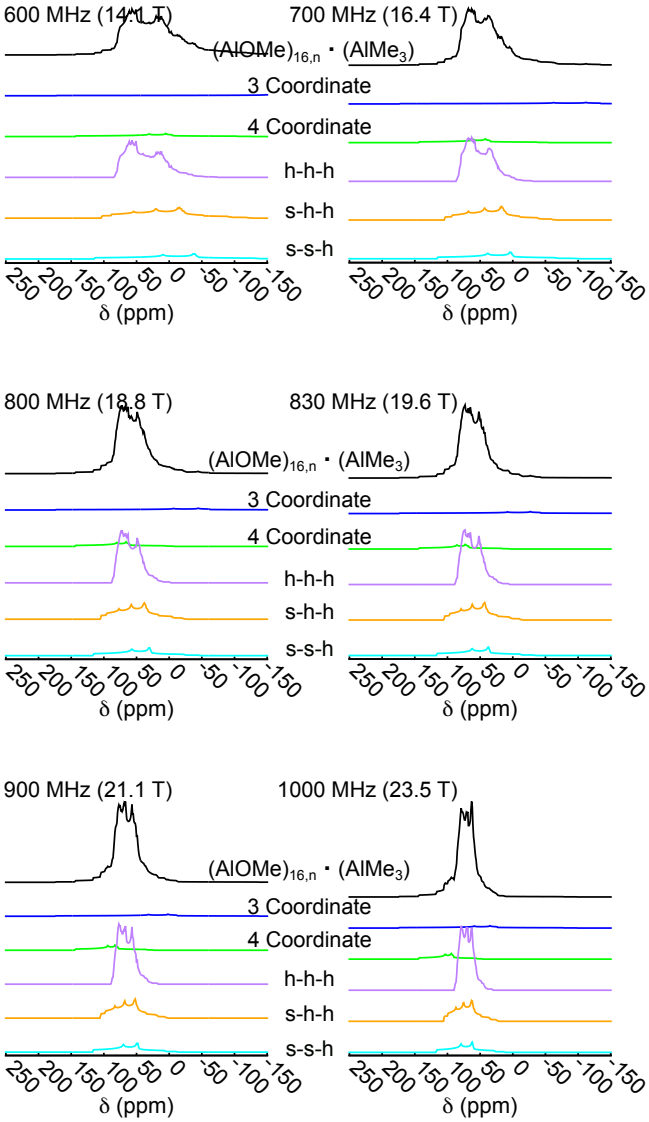

FIG. S86. Calculated EFG parameters and NMR chemical shifts of **(AlOMe)$_{16,t}$**.

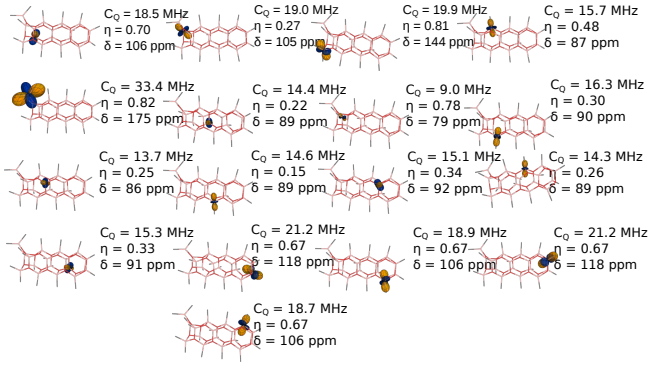

FIG. S87. SSNMR spectra of $\mathbf{(AlOMe)_{16,t} \cdot (AlMe_3)_2}$, simulated at different field strengths (the corresponding proton resonance frequencies are also provided).

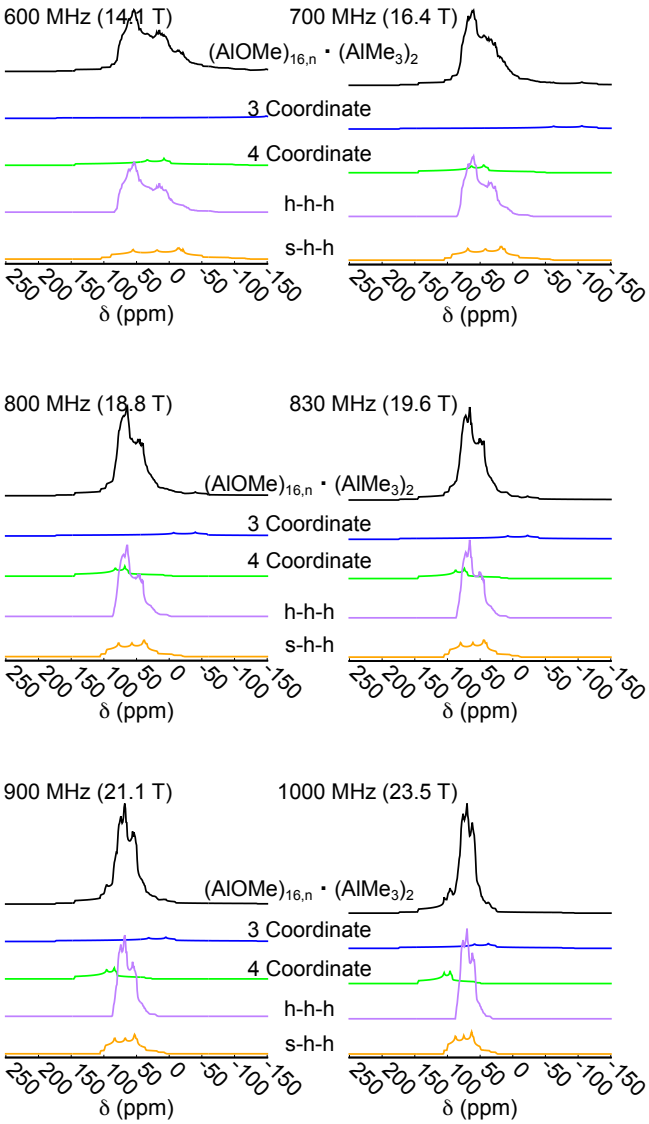

FIG. S88. Calculated EFG parameters and NMR chemical shifts of $\mathbf{(AlOMe)_{16,t} \cdot (AlMe_3)_2}$.

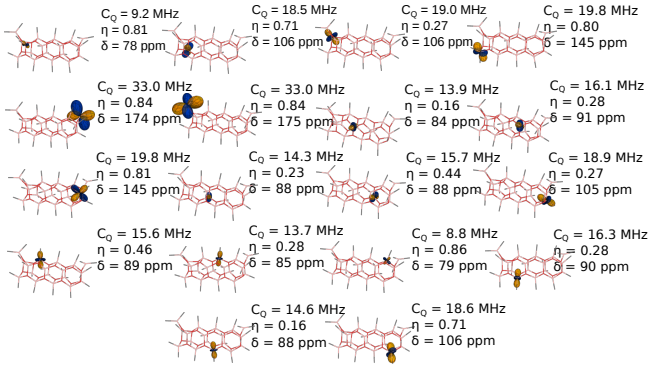

FIG. S89. SSNMR spectra of **(AlOMe)$_{16,t}$ · (AlMe$_3$)$_3$**, simulated at different field strengths (the corresponding proton resonance frequencies are also provided).

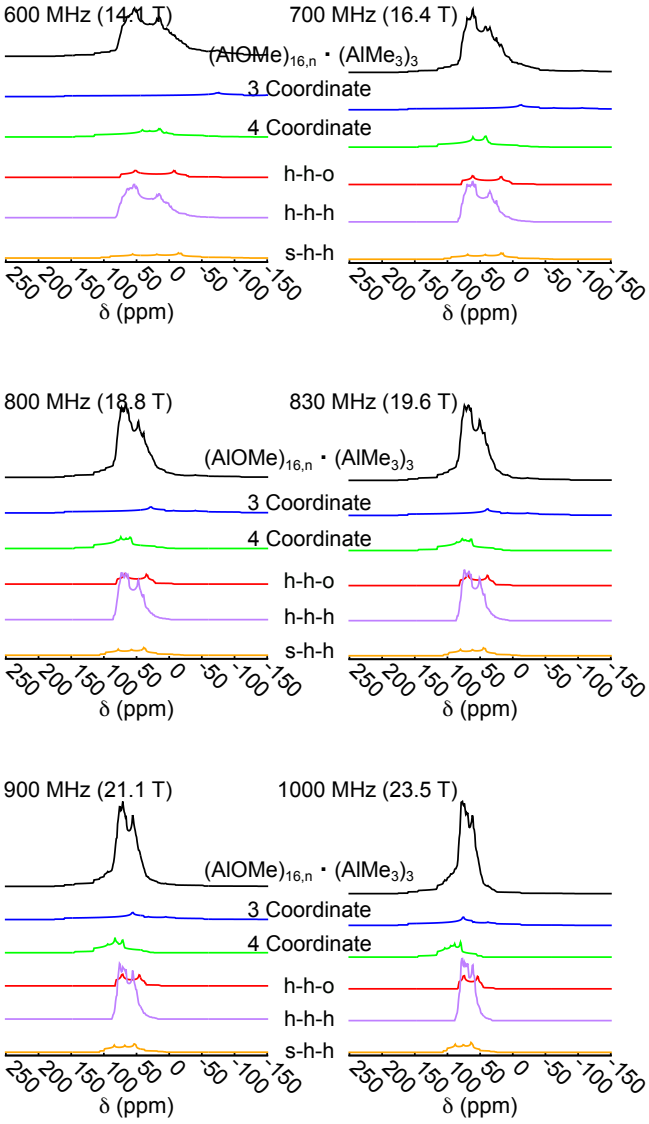

FIG. S90. Calculated EFG parameters and NMR chemical shifts of **(AlOMe)$_{16,t}$ · (AlMe$_3$)$_3$**.

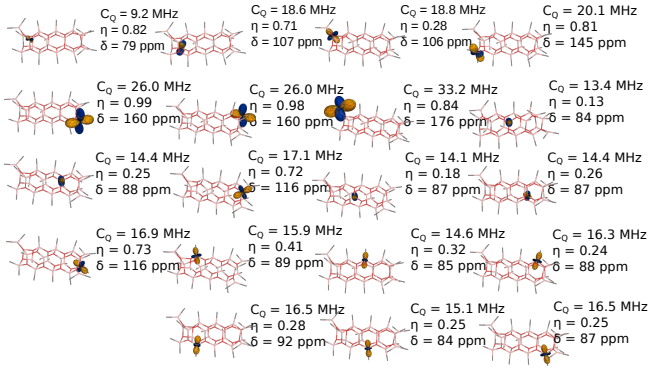

FIG. S91. SSNMR spectra of **(AlOMe)$_{16,t}$ · (AlMe$_3$)$_4$**, simulated at different field strengths (the corresponding proton resonance frequencies are also provided).

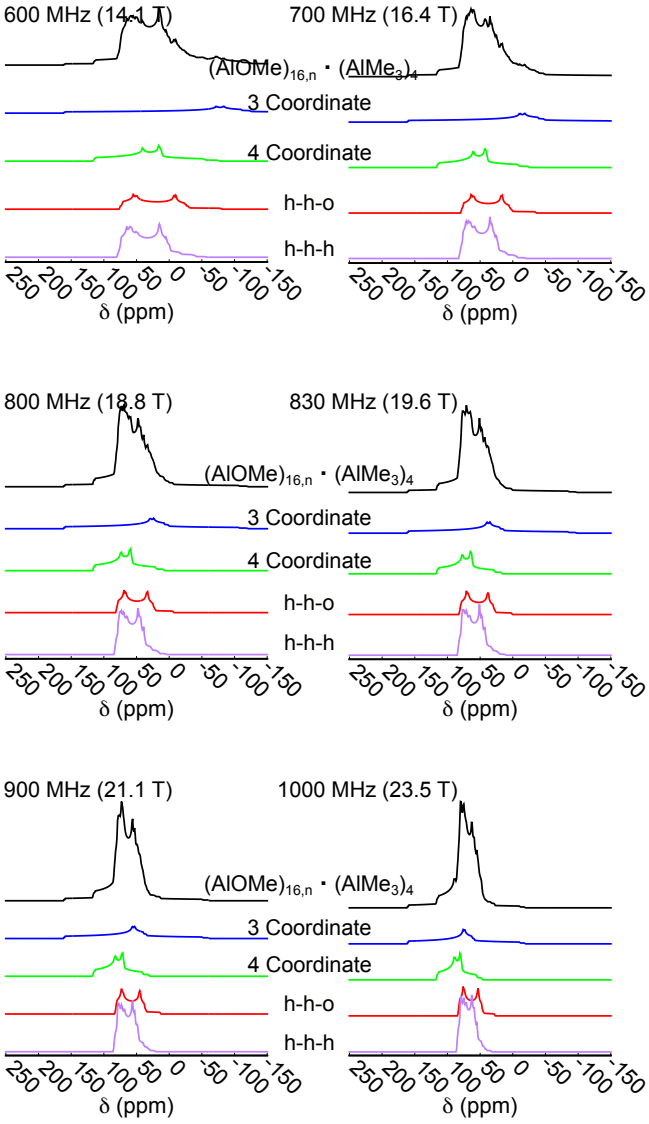

FIG. S92. Calculated EFG parameters and NMR chemical shifts of **(AlOMe)$_{16,t}$ · (AlMe$_3$)$_4$**.

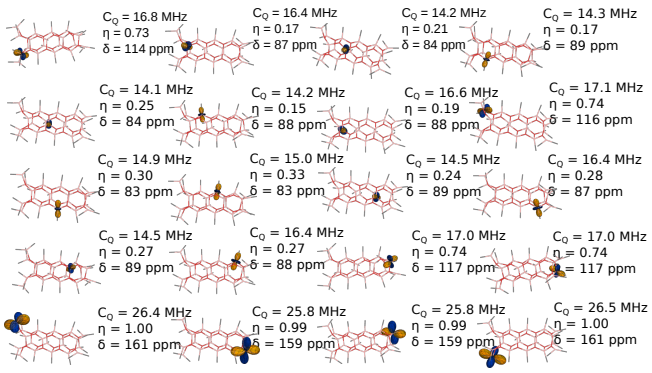

FIG. S93. SSNMR spectra of **(AlOMe)$_{18,t}$**, simulated at different field strengths (the corresponding proton resonance frequencies are also provided).

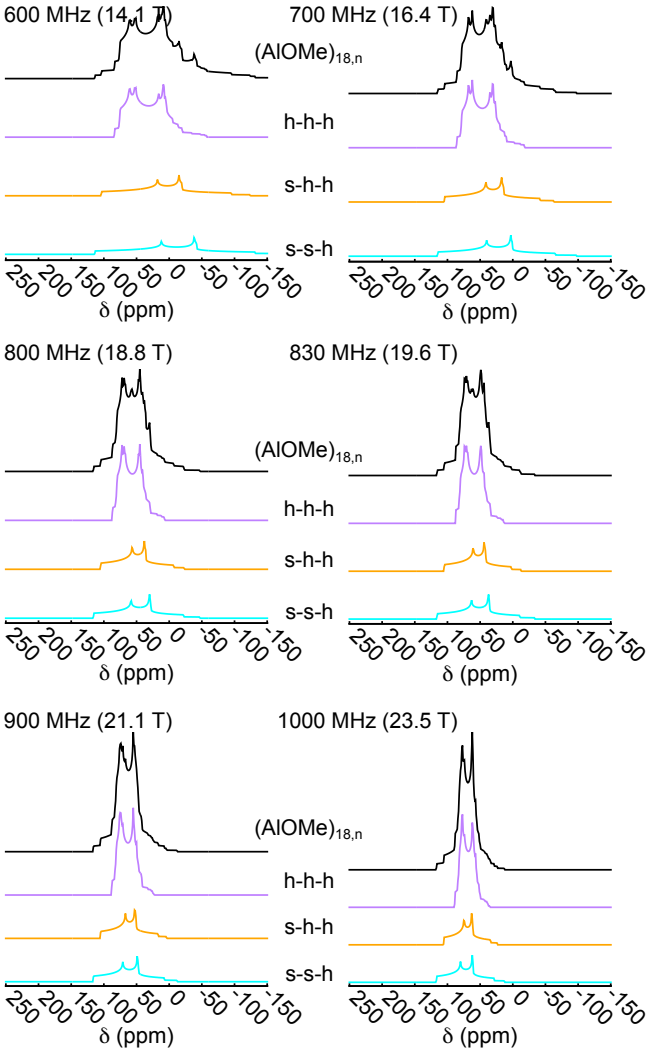

FIG. S94. Calculated EFG parameters and NMR chemical shifts of **(AlOMe)$_{18,t}$**.

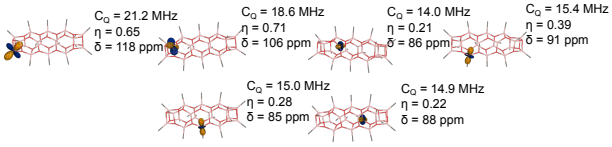

FIG. S95. SSNMR spectra of **(AlOMe)$_{18,t}$ · (AlMe$_3$)**, simulated at different field strengths (the corresponding proton resonance frequencies are also provided).

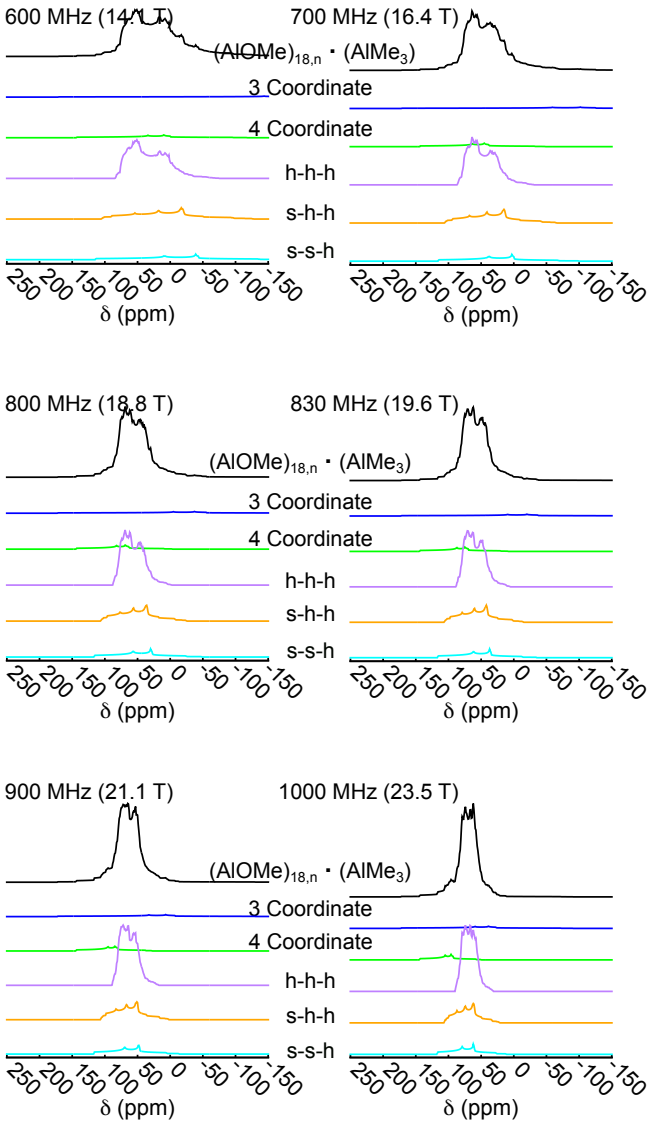

FIG. S96. Calculated EFG parameters and NMR chemical shifts of **(AlOMe)$_{18,t}$ · (AlMe$_3$)**.

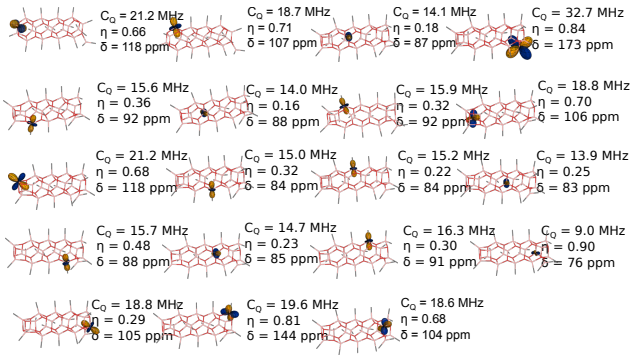

FIG. S97. SSNMR spectra of **(AlOMe)$_{18,t}$ · (AlMe$_3$)$_2$**, simulated at different field strengths (the corresponding proton resonance frequencies are also provided).

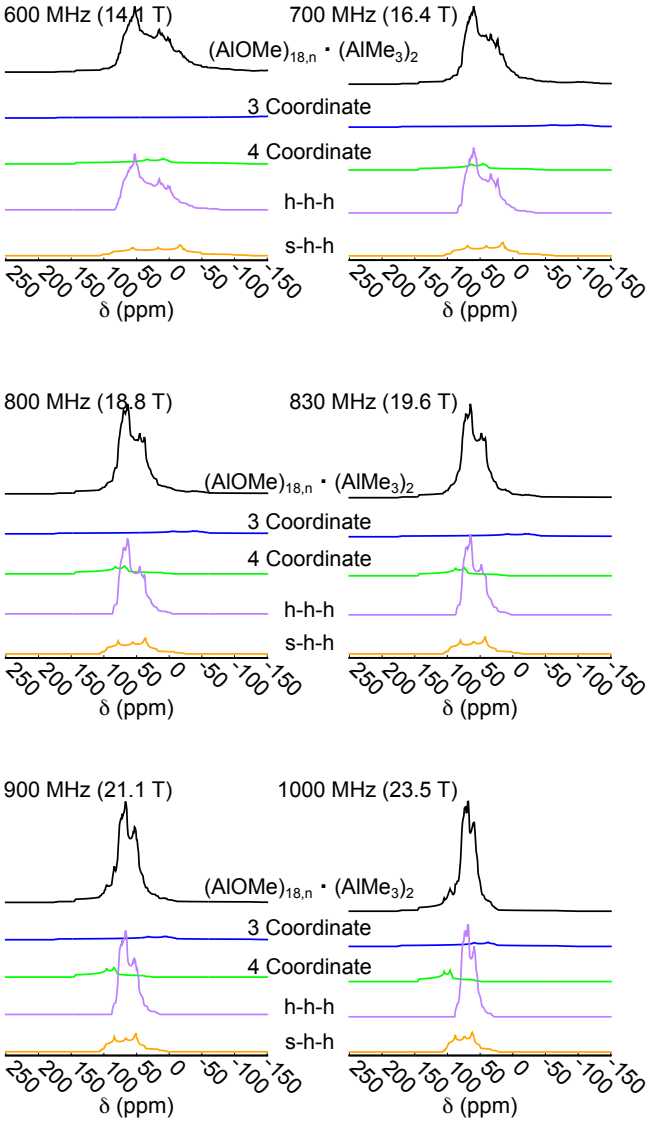

FIG. S98. Calculated EFG parameters and NMR chemical shifts of **(AlOMe)$_{18,t}$ · (AlMe$_3$)$_2$**.

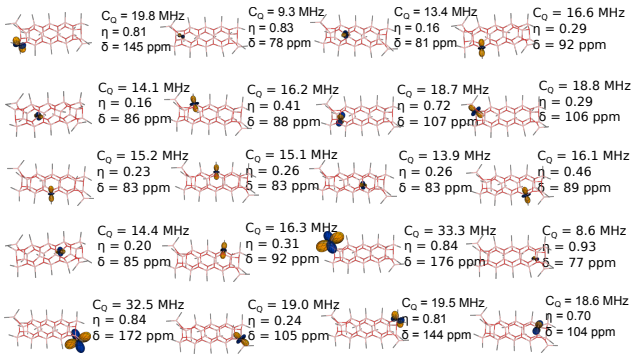

FIG. S99. SSNMR spectra of $\mathbf{(AlOMe)_{18,t} \cdot (AlMe_3)_3}$, simulated at different field strengths (the corresponding proton resonance frequencies are also provided).

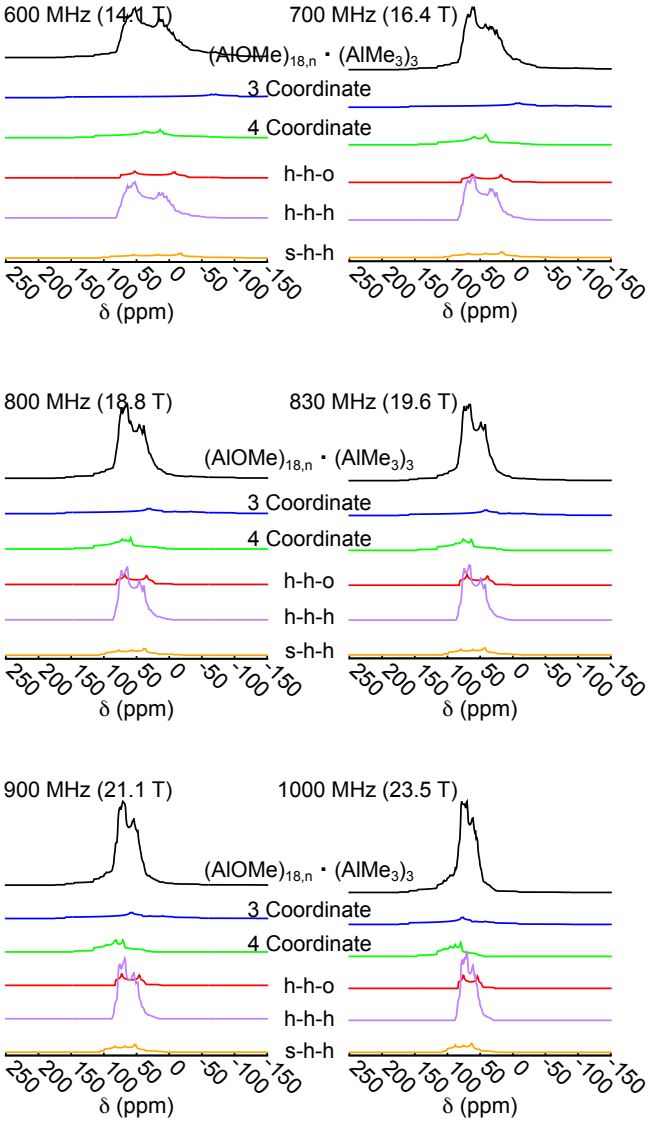

FIG. S100. Calculated EFG parameters and NMR chemical shifts of $\mathbf{(AlOMe)_{18,t} \cdot (AlMe_3)_3}$.

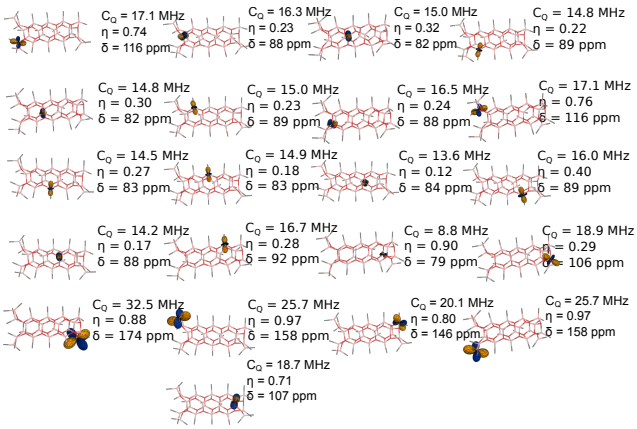

FIG. S101. SSNMR spectra of $\mathbf{(AlOMe)_{18,t} \cdot (AlMe_3)_4}$, simulated at different field strengths (the corresponding proton resonance frequencies are also provided).

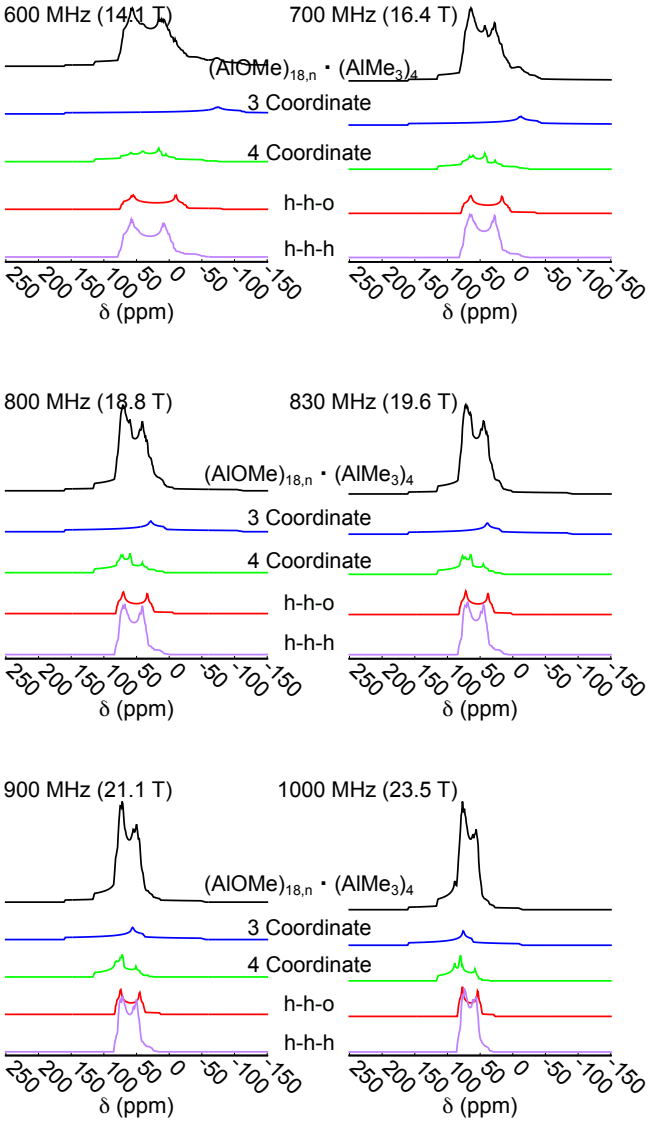

FIG. S102. Calculated EFG parameters and NMR chemical shifts of $\mathbf{(AlOMe)_{18,t} \cdot (AlMe_3)_4}$.

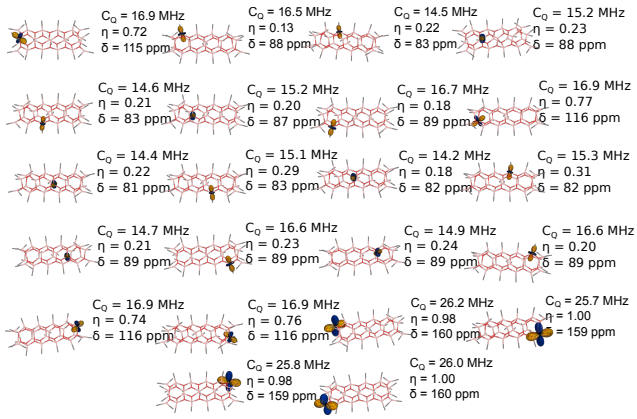

FIG. S103. SSNMR spectra of **(AlOMe)$_{20,t}$**, simulated at different field strengths (the corresponding proton resonance frequencies are also provided).

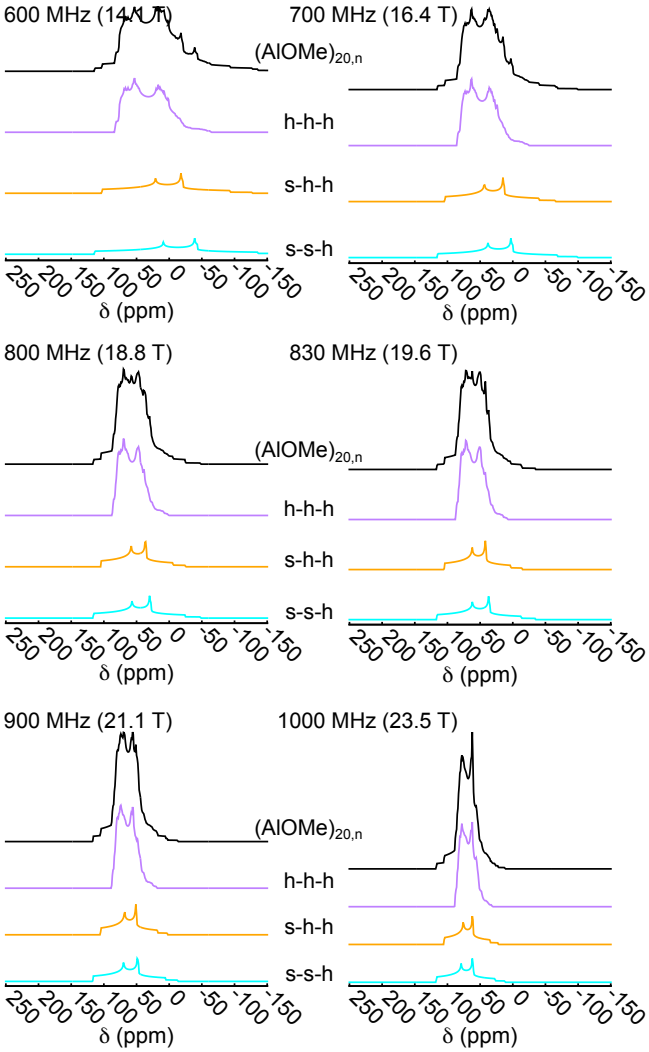

FIG. S104. Calculated EFG parameters and NMR chemical shifts of **(AlOMe)$_{20,t}$**.

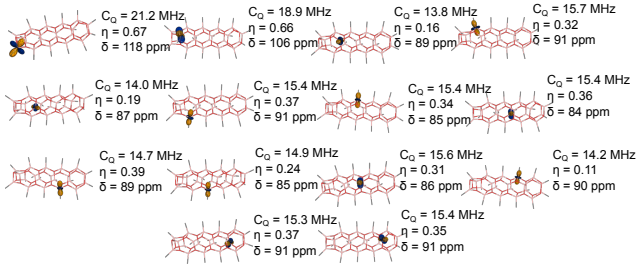

FIG. S105. SSNMR spectra of **(AlOMe)$_{20,t}$ · (AlMe$_3$)**, simulated at different field strengths (the corresponding proton resonance frequencies are also provided).

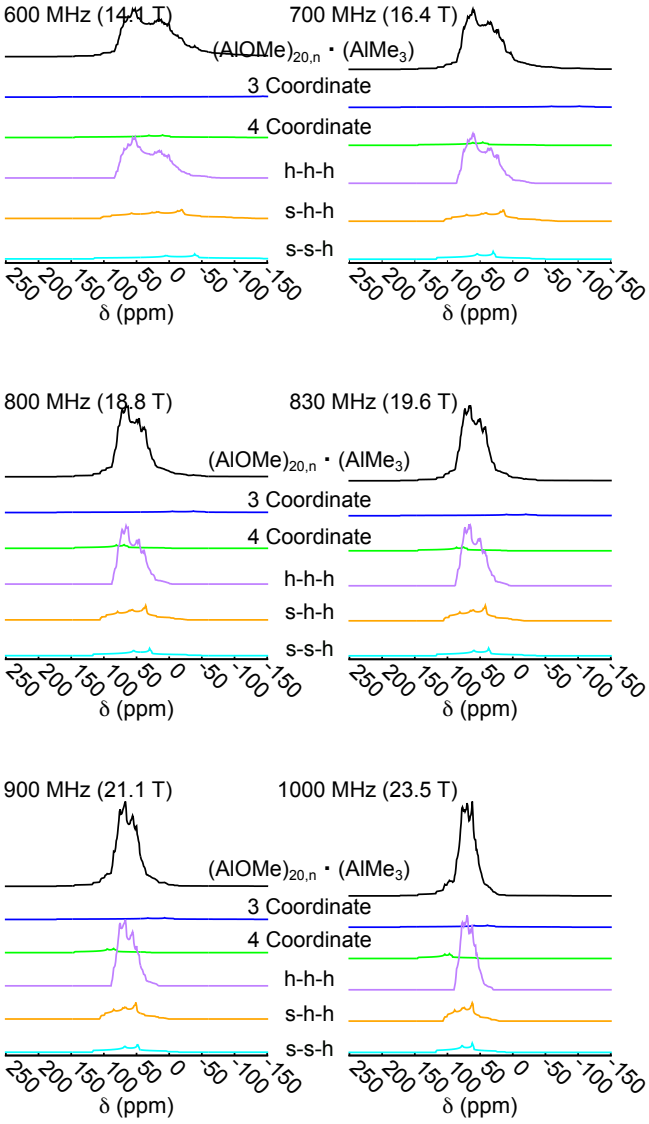

FIG. S106. Calculated EFG parameters and NMR chemical shifts of **(AlOMe)$_{20,t}$ · (AlMe$_3$)**.

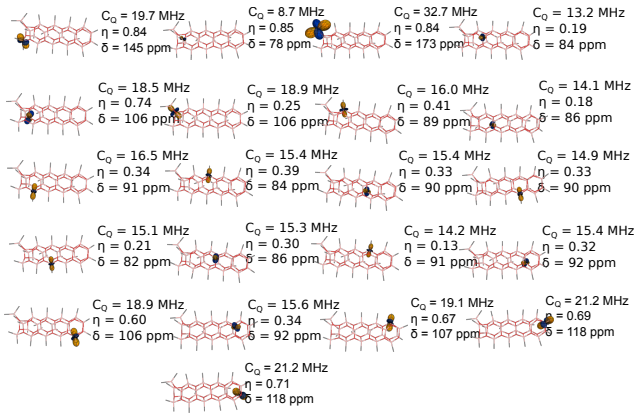

FIG. S107. SSNMR spectra of $\mathbf{(AlOMe)_{20,t} \cdot (AlMe_3)_2}$, simulated at different field strengths (the corresponding proton resonance frequencies are also provided).

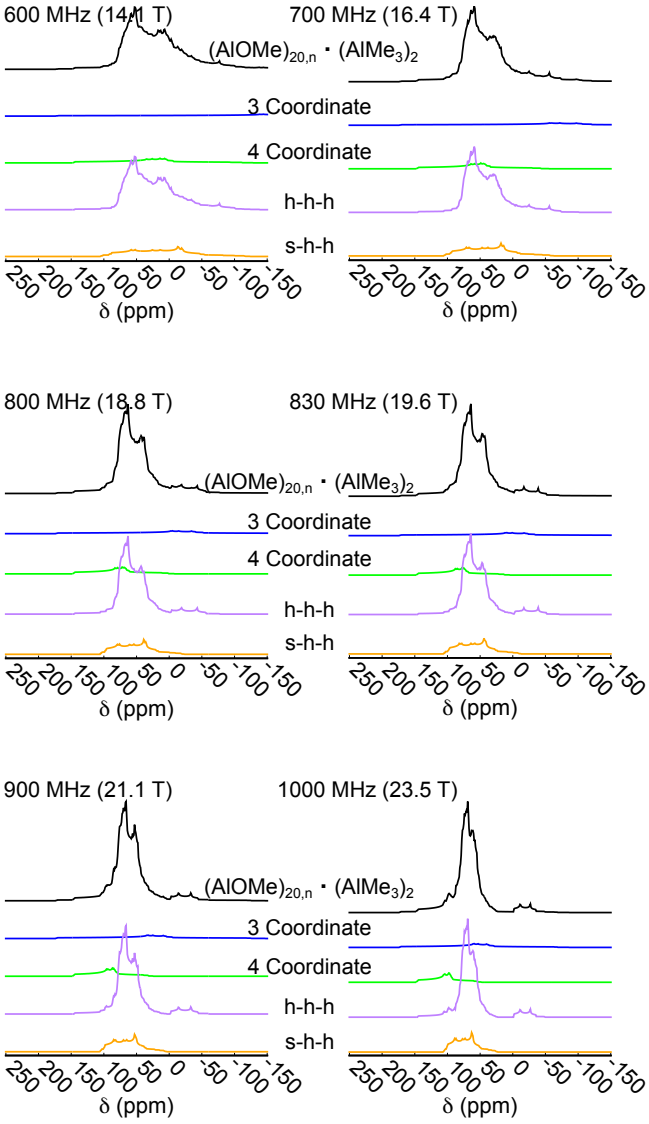

FIG. S108. Calculated EFG parameters and NMR chemical shifts of $\mathbf{(AlOMe)_{20,t} \cdot (AlMe_3)_2}$.

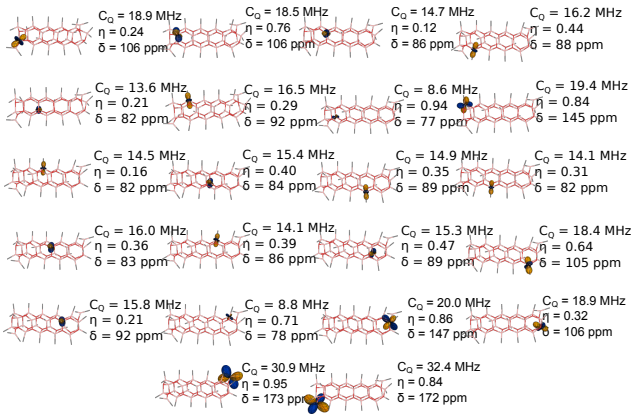

FIG. S109. SSNMR spectra of $\mathbf{(AlOMe)_{20,t} \cdot (AlMe_3)_3}$, simulated at different field strengths (the corresponding proton resonance frequencies are also provided).

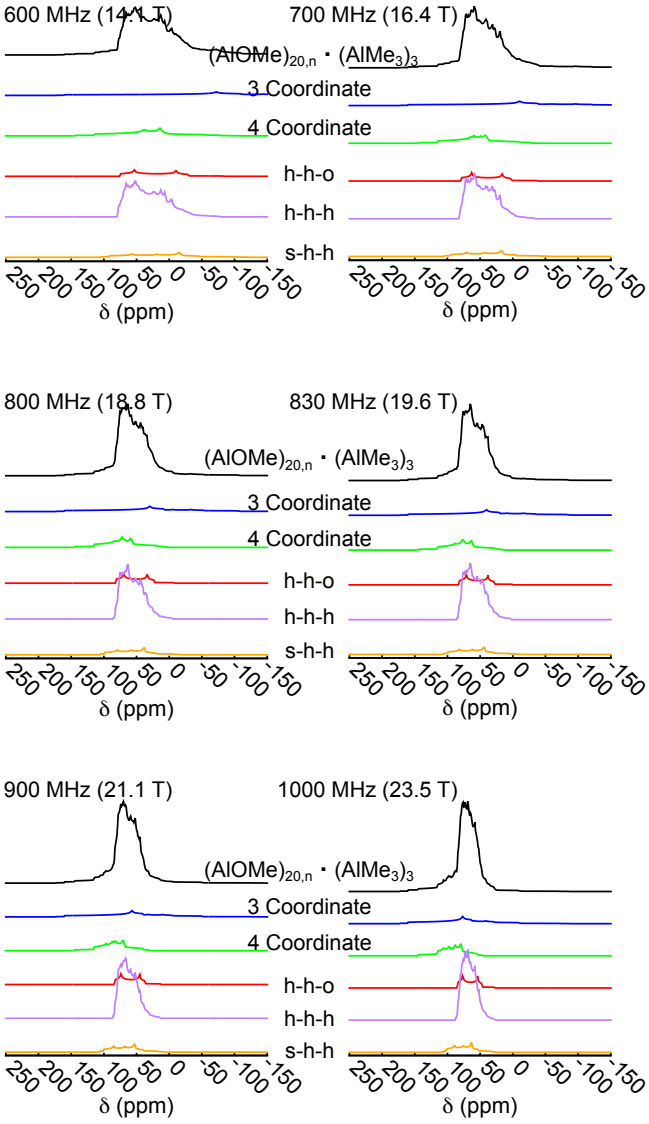

FIG. S110. Calculated EFG parameters and NMR chemical shifts of $\mathbf{(AlOMe)_{20,t} \cdot (AlMe_3)_3}$.

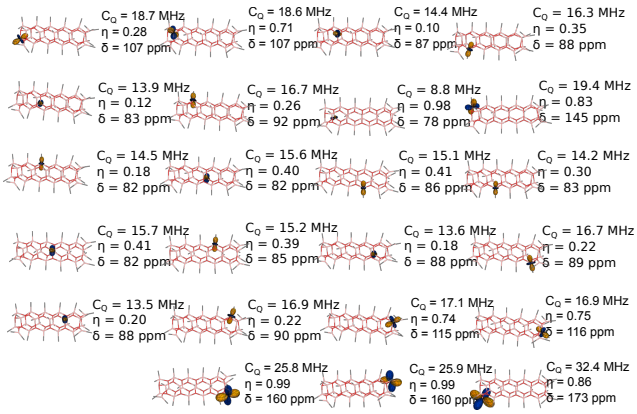

FIG. S111. SSNMR spectra of $\mathbf{(AlOMe)_{20,t} \cdot (AlMe_3)_4}$, simulated at different field strengths (the corresponding proton resonance frequencies are also provided).

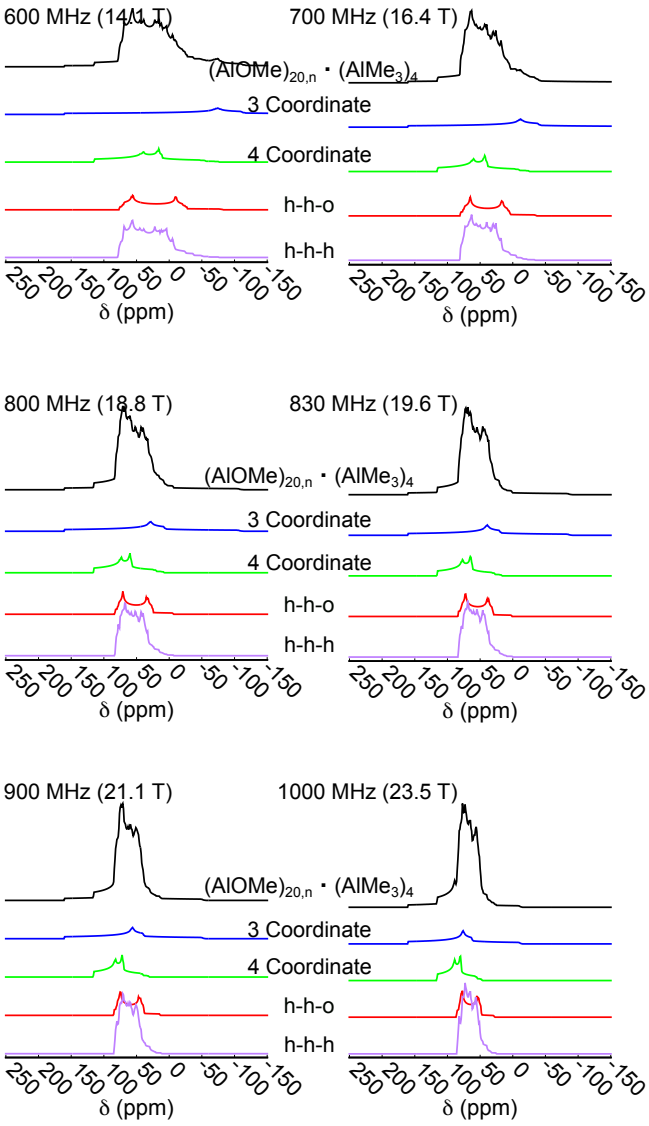

FIG. S112. Calculated EFG parameters and NMR chemical shifts of $\mathbf{(AlOMe)_{20,t} \cdot (AlMe_3)_4}$.